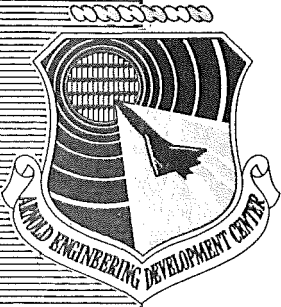


Mills
AEDC-TR-80-1

C.2

B
AUG 17 1981



Effects of Window Configuration on Model Pressure Distribution in Wind Tunnels with Perforated Walls

F. L. Heltsley
ARO, Inc.

January 1981

Final Report for Period October 1978 — September 1979

Approved for public release; distribution unlimited.

Property of Arnold Engineering Development Center
ARO, Inc.
FACCSO-CI-C-0004

ARNOLD ENGINEERING DEVELOPMENT CENTER
ARNOLD AIR FORCE STATION, TENNESSEE
AIR FORCE SYSTEMS COMMAND
UNITED STATES AIR FORCE

NOTICES

When U. S. Government drawings, specifications, or other data are used for any purpose other than a definitely related Government procurement operation, the Government thereby incurs no responsibility nor any obligation whatsoever, and the fact that the Government may have formulated, furnished, or in any way supplied the said drawings, specifications, or other data, is not to be regarded by implication or otherwise, or in any manner licensing the holder or any other person or corporation, or conveying any rights or permission to manufacture, use, or sell any patented invention that may in any way be related thereto.

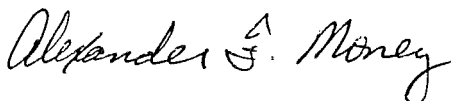
Qualified users may obtain copies of this report from the Defense Technical Information Center.

References to named commercial products in this report are not to be considered in any sense as an indorsement of the product by the United States Air Force or the Government.

This report has been reviewed by the Office of Public Affairs (PA) and is releasable to the National Technical Information Service (NTIS). At NTIS, it will be available to the general public, including foreign nations.

APPROVAL STATEMENT

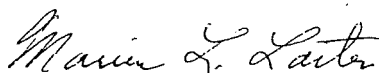
This report has been reviewed and approved.



ALEXANDER F. MONEY
Project Manager
Directorate of Technology

Approved for publication:

FOR THE COMMANDER



MARION L. LASTER
Director of Technology
Deputy for Operations

UNCLASSIFIED

REPORT DOCUMENTATION PAGE		READ INSTRUCTIONS BEFORE COMPLETING FORM
1. REPORT NUMBER AEDC-TR-80-1	2. GOVT ACCESSION NO.	3. RECIPIENT'S CATALOG NUMBER
4. TITLE (and Subtitle) EFFECTS OF WINDOW CONFIGURATION ON MODEL PRESSURE DISTRIBUTION IN WIND TUNNELS WITH PERFORATED WALLS		5. TYPE OF REPORT & PERIOD COVERED Final Report-October 1978 to September 1979
		6. PERFORMING ORG. REPORT NUMBER
7. AUTHOR(s) F. L. Heltsley, ARO, Inc., a Sverdrup Corporation Company		8. CONTRACT OR GRANT NUMBER(s)
9. PERFORMING ORGANIZATION NAME AND ADDRESS Arnold Engineering Development Center/DOT Air Force Systems Command Arnold Air Force Station, Tennessee 37389		10. PROGRAM ELEMENT, PROJECT, TASK AREA & WORK UNIT NUMBERS Program Element 65807F
11. CONTROLLING OFFICE NAME AND ADDRESS Arnold Engineering Development Center/DOS Air Force Systems Command Arnold Air Force Station, Tennessee 37389		12. REPORT DATE January 1981
		13. NUMBER OF PAGES 56
14. MONITORING AGENCY NAME & ADDRESS (if different from Controlling Office)		15. SECURITY CLASS. (of this report) UNCLASSIFIED
		15a. DECLASSIFICATION/DOWNGRADING SCHEDULE N/A
16. DISTRIBUTION STATEMENT (of this Report) Approved for public release; distribution unlimited.		
17. DISTRIBUTION STATEMENT (of the abstract entered in Block 20, if different from Report)		
18. SUPPLEMENTARY NOTES Available in Defense Technical Information Center (DTIC)		
19. KEY WORDS (Continue on reverse side if necessary and identify by block number) <div style="display: flex; justify-content: space-between;"> <div style="width: 45%;"> windows configurations models pressure distribution wind tunnels </div> <div style="width: 45%;"> walls (perforated) transonic flow laser velocimeters Mach numbers flow fields </div> </div>		
20. ABSTRACT (Continue on reverse side if necessary and identify by block number) Larger optical windows for access to the model flow field in the Arnold Engineering Development Center (AEDC) transonic wind tunnels will be required for optimum utilization of the laser velocimeter (LV). A combined analytical and experimental investigation was performed to assess the effects of such windows upon the performance of the perforated walls. The experimental		

UNCLASSIFIED

UNCLASSIFIED

20. ABSTRACT (Continued)

results from the Aerodynamic Wind Tunnel (1T) indicate that although the wall interference characteristics of some window configurations approach the standard porous wall, none of the configurations tested exhibited adequate wave cancellation for all Mach numbers from $M_{\infty} = 1.0$ through 1.4. A variable porosity wall arrangement is described which appears to be capable of providing acceptable optical access without adversely affecting the tunnel flow field.

UNCLASSIFIED

PREFACE

The work reported herein was conducted by the Arnold Engineering Development Center (AEDC), Air Force Systems Command (AFSC), and Alex F. Money was the Air Force project manager. The results were obtained by ARO, Inc., AEDC Division (a Sverdrup Corporation Company), operating contractor for the AEDC, AFSC, Arnold Air Force Station, Tennessee, under ARO Project No. P32C-36C. The manuscript was submitted for publication on December 3, 1979.

CONTENTS

	<u>Page</u>
1.0 INTRODUCTION	5
2.0 ANALYTICAL STUDY	
2.1 Mathematical Modeling	5
2.2 Wall Interference Calculations	6
2.3 Conclusions	7
3.0 EXPERIMENTAL INVESTIGATION	
3.1 Wind Tunnel Facility	8
3.2 Test Articles	8
3.3 Wall Configurations	8
3.4 Test Conditions	9
3.5 Cone/Cylinder Results	9
3.6 Wing/Centerbody Results	12
4.0 CONCLUDING REMARKS	12
REFERENCES	13

ILLUSTRATIONS

Figure

1. Vortex Lattice Representations of a Wind Tunnel Sidewall	15
2. Sidewall Configurations for Analytical Study	16
3. Comparison of Present Method and Point-Matching Technique (Ref. 3)	17
4. Distribution of Lift Interference Factor and Wake Blockage Ratio along Wind Tunnel Centerline for Several Wall Configurations	19
5. Interference Velocity Vector Projections on Constant x-Planes Resulting from a Unit Source (Wake Blockage Disturbance) at $x = 0$	25
6. Interference Velocity Vector Projections on Constant x-Planes Resulting from a Unit Vortex ($\zeta = 0.667$) (Lift Disturbance) at $x = 0$	29
7. Test Models	33
8. Installation in Tunnel 1T	34
9. Sidewall Configurations Tested	35
10. Modification of Tunnel 1T Standard Sidewalls	36

<u>Figure</u>	<u>Page</u>
11. Axial Distribution of Pressure Coefficient on Cone/Cylinder for Configuration 300 and Mach Numbers from 0.5 through 1.4	37
12. Axial Distribution of Pressure Coefficient on Cone/Cylinder for Selected Wall Configurations and Mach Numbers	39
13. Axial Distribution of Pressure Coefficient on Cone/Cylinder for Selected Wall Configurations and Mach Numbers above 1.0	48
14. Distribution of Pressure Coefficient on the Wing and Centerbody for Selected Wall Configurations and Mach Numbers	50
15. Variation of Normal-Force Coefficient with Mach Number, Nominal $\alpha = 4$ deg	54
NOMENCLATURE	55

1.0 INTRODUCTION

Visual access to the model flow field is severely restricted in most wind tunnels having perforated walls. Optimum use of the laser velocimeter (LV) will require an increase in viewing area. The purpose of this investigation was to evaluate the performance of several window configurations relative to the standard six-percent perforated wall liners in the Arnold Engineering Development Center (AEDC) Aerodynamic Wind Tunnel (1T). The general criteria for an acceptable optical wall arrangement were chosen as (1) that the wall contain a window with a length approximately equal or equal to the test section height and with a height of one-half its length, and (2) that the optical wall arrangement produces interference in the model flow field at least as low as that resulting from use of the standard six-percent perforated wall.

2.0 ANALYTICAL STUDY

2.1 MATHEMATICAL MODELING

Candidate window configurations were selected for testing based upon a subsonic inviscid wall interference analysis using the Augmented Potential Flow Program (APFP) described in Refs. 1 and 2.

A horseshoe vortex and a source were used in the calculation of lift and blockage interference, respectively. Choice of a source to represent model body blockage rather than a doublet was based upon the characteristics of the experimental models to be tested. For consistency with the literature, the blockage will hereafter be referred to as wake blockage even though it represents the test article "body" and supporting sting.

Each wind tunnel test section wall was represented by a rectangular array of vortex panels. The two kinds of arrays, shown in Fig. 1, were formulated to provide configuration flexibility. By specifying the value of the porosity parameter (Q) at the control point of each individual panel, any desired porosity distribution could be imposed. The sidewall configurations investigated are illustrated in Fig. 2. Window areas (solid), $Q = 0$, appear in black, whereas different types of crosshatching are used to indicate other porosity values. The panels with $Q = 0.3$ represent solid taper or transition regions to minimize disturbances associated with abrupt changes in porosity (see Fig. 8). All but one of the configurations shown were combined with standard upper and lower walls with $Q = 0.5$. Configuration 1 was a closed tunnel with $Q = 0$ on all four walls.

Potential flow solutions were obtained by specifying the strength of either the source or vortex representing the test article disturbance, imposing the desired individual wall panel boundary conditions, and solving for the wall panel singularity strengths as in Refs. 1 and 2.

2.2 WALL INTERFERENCE CALCULATIONS

Having solved for the wall panel singularity strengths, one may compute the wall interference at any point by summing the velocity components induced at that point by all of the wall singularities. The axial distributions of the wall interference factor, δ , and the wake blockage ratio, Ω_w , were calculated for each configuration in Fig. 2. Distributions obtained for configuration 3 ($Q = 0.5$ on all walls) are compared well with the point-matching results from Ref. 3 in Fig. 3. The slight discrepancy in lift interference factor is consistent with the vortex span effect discussed in Ref. 4; therefore, configuration 3 was used as a basis for comparisons for the window configurations. A higher porosity would reduce the blockage interference but would result in an increased lift interference. A lower porosity would have the opposite effect.

Selected streamwise interference distributions are compared in Fig. 4 to illustrate the effects of wall configuration. The distributions computed for four different window lengths and a fixed leading edge are presented in Fig. 4a. The results for all four windows were so similar that only one curve could be drawn. The effect of window position is more pronounced as shown in Fig. 4b, especially upon the wake blockage ratio upstream of the disturbance. The interference remains relatively constant downstream of the disturbance. Centering the window on the disturbance produces the lowest lift interference and the highest wake blockage ratio at that station, $x/\beta b = 0$. The opposite effect can be seen if the window is moved either upstream or downstream.

Computed wall interference results for three different size windows, with and without leading- and trailing-edge transition regions, are presented in Figs. 4c, d, and e. Included for comparison are the configuration 3 distributions. In each case, the addition of a window improves lift interference but has an adverse effect on wake blockage ratio since such a wall modification lowers the average wall porosity. The small changes in the distribution of interference caused by the transition regions are similar to those observed in Fig. 4b and appear to be related to effective translation of the window leading edge. This hypothesis is verified in Fig. 4e which shows that the leading-edge transition is responsible for a majority of the difference in distribution with and without transition.

In order to add a sidewall window without significantly increasing the wall interference above the configuration 3 levels, it seems reasonable to assume that additional flow relief in the vicinity of the window would be beneficial. Configuration 6 was designed to provide a constant local average porosity of approximately $Q = 0.5$ at any station along the tunnel axis. This was accomplished by placing 3- by 12-in. panels having a porosity of $Q = 0.6$ above and below the 6- by 12-in. window where $Q = 0$. The resulting interference

distributions are compared in Fig. 4f with computed results for configurations 3 and 5. The effects of the $Q = 0.6$ panels (configuration 6) are seen to nearly cancel the effects of the window (configuration 5) at the $x/\beta b = 0$ station to yield both lift and wake blockage interference levels which are near those of configuration 3. The configuration 6 wake blockage ratio distribution is different from that of configuration 3, however, with configuration 6 providing a more favorable gradient in the vicinity of the disturbance.

In addition to the axial distribution of the lift and wake blockage interference factors on the tunnel centerline, the vortex lattice technique was also used to compute interference velocities at other locations within the test section. Projections of the interference velocity vectors onto constant x-planes are shown in Figs. 5 and 6 for wake blockage and lift disturbances, respectively. The method of presenting interference data gives a direct graphical representation of sidewash and upwash velocities resulting from such disturbances and can yield valuable insight into the three dimensionality of the flow patterns.

The flow fields for the first three configurations of Fig. 5 are quite different. As can be seen, configuration 3 does a remarkable job of reducing the interference throughout the test section. The large lateral disturbances reappear with the addition of the window in both configurations 5 and 6 and could result in relatively large errors for tests involving large span test articles.

The high level of upwash interference in the plane of the lift disturbance for the closed tunnel (configuration 1) shown in Fig. 6a is consistent with the lift interference factor data presented earlier in Fig. 3a. The significant reduction of downwash resulting from perforating the walls is illustrated in Figs. 6a and b. The relative insensitivity of lift interference to differences in sidewall can be seen by comparing Fig. 4b with c and d. Only slight changes in the gradient of downwash along the wing span can be seen between the three latter configurations.

2.3 CONCLUSIONS

Based upon the subsonic analysis, sidewall windows can be used as long as a six-percent average wall porosity is maintained at any axial station and there are no significant crossflows generated in the vicinity of the test article. It can be shown that a slight reduction in the average porosity below the standard six percent will produce a lower level of lift interference since the standard walls are too open for complete cancellation of the interference. Such a change in porosity, however, will result in an increase of wake blockage. A slight increase in the average porosity will produce the opposite effects on both lift and blockage interference.

3.0 EXPERIMENTAL INVESTIGATION

3.1 WIND TUNNEL FACILITY

The experiments described herein were performed in the AEDC Tunnel 1T (Ref. 5). The facility can provide continuous flow at Mach numbers from 0.2 through 1.5. The 12-in.-square test section is 37.5 in. long and is formed by four removable walls. The upper and lower walls are adjustable to permit variation of wall angle. For the standard P29 wall configuration, all four wall liners are perforated with 0.125-in.-diam holes inclined into the airstream at an angle of 60 deg to provide a six-percent open area.

3.2 TEST ARTICLES

The two test articles illustrated in Fig. 7 have been used extensively in the investigation of lift and blockage interference caused by wind tunnel walls. The cone/cylinder (Fig. 7a) was used in early experiments to evaluate perforated walls and in the development of the differential resistance wall configuration presently used in the AEDC transonic wind tunnels (Refs. 6 through 12). The wing/centerbody (Fig. 7b) has been used as a standard model for the evaluation of lift interference (Ref. 13). Although most of the previous experiments involved a dual lifting surface (wing and tail), the wing alone was used in the subject test. The installation of each test article in Tunnel 1T is shown in Fig. 8.

The wing was equipped with pressure orifices at the mid-semispan location. Nineteen taps were distributed chordwise along the upper surface of the right wing. A similar number were installed on the lower left wing surface. In addition, two axial rows of eleven orifices each were located on the centerbody, one row on the upper centerline and another on the lower centerline. The wing/centerbody sting was equipped with two sets of strain gages, calibrated to provide the normal force and moment acting on the model.

Forty-four orifices were installed in a single axial row along the upper-surface centerline of the cone/cylinder.

3.3 WALL CONFIGURATIONS

The twelve sidewall configurations selected for experimental evaluation are illustrated in Fig. 9. Configuration 300 is the standard P29 sidewall liner having a nominal six-percent porosity. Configuration 600 was obtained by the modification of configuration 300 shown schematically in Fig. 10. The remaining 600 series as well as the 500 series configurations were prepared by filling appropriate holes with water putty.

3.4 TEST CONDITIONS

Surface pressure data were obtained for Mach numbers from $M_\infty = 0.5$ through 1.4 for both models. The cone/cylinder was tested in conjunction with all the Fig. 9 wall configurations using the optimum wall schedule, $\theta_w = \theta_w^*$ (Ref. 12). Additional cone/cylinder measurements were made for configurations 300, 600, 601, and 602 using $\theta_w = 0$. The wing/centerbody was tested with wall configurations 300, 511, 600, 601, 602, and 522 using $\theta_w = \theta_w^*$. No wing/centerbody measurements were made with $\theta_w = 0$.

3.5 CONE/CYLINDER RESULTS

The distribution of pressure coefficient along the upper surface of the cone/cylinder is presented in Fig. 11 for configuration 300 at Mach numbers from $M_\infty = 0.5$ through 1.4. Measurements, for both zero wall, $\theta_w = 0$, and optimum wall, θ_w^* , are included for each Mach number. It appears that the wave cancellation properties of the wall are sensitive to changes in wall angle as evidenced by the significant differences in the model pressure distribution where the optimum wall setting is not zero degrees. This is consistent with the statement in Ref. 8 that wall angle can significantly affect the compression and expansion cancellation properties of a perforated wall.

The ability of a wind tunnel wall to cancel test-article-generated disturbances is strongly dependent upon the distribution of porosity. Model surface pressure measurements obtained for the cone/cylinder are presented in Fig. 12 to illustrate the effects of sidewall configurations. Theoretical pressure distributions computed using two techniques described in Refs. 9 and 14 are included for comparison.

The extremes of the experimental configurations are presented in Fig. 12a. The configuration 600 results are similar to those presented in Ref. 8 for a “too open” wall, whereas the configuration 511 distribution suggests a “too closed” boundary. The configuration 300 walls provide a marked reduction in interference. Apparently the bow shock was reflected as a weak expansion intercepted by the model at $x_c/D = 4.0$. The increase in pressure coefficient which follows $x_c/D = 4.0$ to 6.0 resulted from the cone compression field being reflected by the wall as a compression. No shoulder expansion can be seen.

Pressure distributions for three different window lengths are presented in Fig. 12b. Since the trailing edge of each window was at the same axial station, any decrease in length resulted in a downstream translation of the leading edge. The medium length window, configuration 522, caused little improvement over configuration 511 since both windows extended far enough upstream to intercept the bow shock. The shock apparently struck the

wall upstream of the short window, configuration 525, resulting in a pressure distribution similar to that of configuration 300 from the nose to $x_c/D = 7.0$. The data at $x_c/D = 7.0$ to 8.0 indicate that the aft portion of the shoulder expansion was intercepted by the window and reflected as an expansion.

Configuration 527 was tested to separate the effects of window length and leading-edge position. A window slightly shorter than the configuration 525 case was positioned so that its leading edge corresponded to that of the configuration 511 window. The three resulting model pressure distributions are compared in Fig. 12c. The bow shock and the forward portion of the cone compression were reflected in the same manner by configurations 511 and 527. The perforated wall aft of the configuration 527 window, however, provided insufficient restriction to the outflow induced by the high-pressure region downstream of the reflected shock. As a result, a secondary expansion system was generated impinging on the model at $x_c/D = 5.0$. The remainder of the distribution indicates that the shoulder expansion was adequately cancelled.

A similar secondary (wall-generated) disturbance originated near the leading edge of the configuration 525 window at $M_\infty = 1.4$. At that Mach number, flow leaves the test section through the porous wall between the bow shock and the window to relieve the overpressure from the shock and model nose flow field. The effect of the secondary compression on the model pressure distribution resulting from the abrupt change of porosity and associated reduction in outflow can be seen from $x_c/D = 7.0$ to 8.0 in the second part of Fig. 12c.

Placing a transition region upstream of configuration 525 results in the distribution presented in Fig. 12d for configuration 524. Two effects of the transition appear at $M_\infty = 1.4$. The increase in resistance to outflow immediately upstream of the window significantly reduces the strength of the secondary compression. The more closed wall, however, reflects the bow shock and nose compression field as a slight compression rather than the slight expansion seen in the configuration 300 distribution.

At $M_\infty = 1.2$ the reflected shoulder expansion is nearly as strong as that produced by the medium length window, configuration 522, in Fig. 12b. In addition, the transition region tends to exaggerate the effect of the nose compression producing a higher peak pressure at $x_c/D \approx 0.6$ than did the largest window, configuration 511, in Fig. 12b.

Replacing a solid window with alternating closed and six-percent perforated lateral strips yields a somewhat limited visual access to an area with the same outer dimensions as the solid window. Coupled with vertical translation of the test article, such a configuration can provide access to the entire region. Model pressure distributions for solid and strip windows

are compared in Figs. 12e and f. The secondary compression which was indicated by the Fig. 12c distribution for the aft window, configuration 526, at $M_\infty = 1.4$ was significantly reduced by a strip window at the same position. The distribution presented in Fig. 12c also indicates a reduction in the strength of the shoulder expansion reflection from the window. The strip window in the forward position, configuration 528, served to reduce the secondary expansion effect observed in Fig. 12c for configuration 527 at $M_\infty = 1.2$. The configuration 528 window had little effect on the reflection of the bow shock and nose compression field at that Mach number. The resulting model pressure distribution presented in Fig. 12f is actually closer to the analytical interference-free solutions than are the configuration 300 data.

Configurations 601 and 602 were designed for experimental investigation of the constant average porosity concept which produced the most promising results in the analytical investigation. The two wall arrangements were intended to produce "large-" and "small-grain" effects, respectively, with the latter configuration providing a more even distribution of porosity in the vertical direction. In both cases the sidewalls in the vicinity of the model consisted of panels having zero (window), six- and twelve-percent porosity with each value of porosity covering a total of one-third of the wall height. As can be seen in Fig. 12g, the cone/cylinder pressure distributions for both configurations correlate well with the configuration 300 data at $M_\infty = 1.2$.

Comparisons of the cone/cylinder distributions for configurations 300 and 511 with configurations 601 and 602 are presented in Fig. 13 for selected Mach numbers above 1.0. Configuration 602 exhibits somewhat better wave cancellation characteristics than does configuration 601, but the slight reduction in interference does not justify segmentation of the window.

Figure 13b shows that the distributions generated by configurations 601 and 300 correlate well at the Mach numbers above $M_\infty = 1.15$. The distributions at $M_\infty = 1.05$ and 1.1 indicate, however, that configuration 601 was "too open" under those flow conditions. The close agreement between the distributions of configurations 300 and 511 at the latter two Mach numbers strengthens the hypothesis, since configuration 601 is basically the same as configuration 511, except with panels of twelve-percent porosity added above and below the window. Good correlation with the standard six-percent walls can thus be obtained with either configuration 601 or 511 at each Mach number in the range from $M_\infty = 1.05$ through 1.4. Therefore, it seems reasonable to conclude that similar wave cancellation characteristics could be achieved at all the same Mach numbers with a single wall arrangement having variable porosity panels above and below the configuration 601 window.

3.6 WING/CENTERBODY RESULTS

Experimental chordwise distributions of surface pressure along the wing and centerbody are presented in Figs. 14a, b, and c for selected configurations and test conditions. Although significant differences in the distribution of pressure resulted from variation of angle of attack and Mach number, changes caused by modification of the tunnel walls were nearly negligible. The experimental measurements for configuration 300 in Figs. 14a and b show, respectively, the effects of angle of attack and Mach number. To illustrate the relative magnitude of pressure distribution variation associated with the sidewall arrangement data representing the two extremes, namely configuration 511 (too closed) and configuration 600 (too open), are presented with the configuration 300 results for $M_\infty = 1.2$ and $\alpha_c = 4.0$ deg in Fig. 14c. The comparatively small differences observed in the distributions appear to have resulted from minor variations in model attitude and tunnel flow condition thought to be within the tolerances specified for the tunnel instrumentation. Normal-force coefficient for a nominal angle of attack of 4 deg is presented versus Mach number in Fig. 15. Measurement uncertainty based upon an error analysis using the estimated individual error levels is represented by vertical bars in the same figure. Since most of the experimental data for all configurations fall within the computed error band, any apparent trend at a given Mach number would be of questionable origin. It is reasonable to conclude that no significant changes in lift interference were caused by any of the wall configurations tested.

4.0 CONCLUDING REMARKS

The results of this study to determine a suitable window/wall configuration indicate that lift and blockage interference were negligible for all of the window arrangements tested throughout the subsonic Mach number range. For supersonic Mach numbers the wave cancellation properties of certain configurations were found to approach the characteristics of the standard porous wall with no windows. No single window arrangement that was tested satisfies the general criterion of providing both low interference and unimpeded optical access to the test article flow field for all Mach numbers.

Based on this test, it seems unlikely that the stated criterion can be satisfied by a passive window/wall. However, the data indicate that adequate cancellation of model-generated compression and expansion waves at all Mach numbers between $M_\infty = 1.0$ and 1.4 could be provided by an arrangement consisting of a 6- by 16-in. window with a 3- by 16-in. variable porosity panel above and below.

REFERENCES

1. Todd, D. C. and Palko, R. "The AEDC Three-Dimensional, Potential Flow Computer Program, Vol. I. Method and Computer Program." AEDC-TR-75-75 (ADA021693) February 1976.
2. "A Vortex Lattice Technique for Computing Ventilated Wind Tunnel Wall Interference." AEDC-TR-79-21 (ADA070445), June 1979.
3. Lo, C. F. and Oliver, R. H. "Boundary Interference in a Rectangular Wind Tunnel with Perforated Walls." AEDC-TR-70-67, (AD704123), April 1970.
4. Kraft, E. M. "Upwash Interference on a Symmetrical Wing in a Rectangular Ventilated Wall Wind Tunnel: Part I - Development of Theory." AEDC-TR-72-187 (AD757196), March 1973.
5. *Test Facilities Handbook* (Eleventh Edition). "Propulsion Wind Tunnel Facility, Vol. 4." Arnold Engineering Development Center, June 1979.
6. Gray, J. D. and Gardenier, H. E. "Experimental and Theoretical Studies on Three-Dimensional Wave Reflection in Transonic Test Sections - Part I: Wind Tunnel Tests on Wall Interference of Axisymmetric Bodies at Transonic Mach Numbers." AEDC-TN-55-42 (AD82559), March 1956.
7. Chew, W. L. "Experimental and Theoretical Studies on Three-Dimensional Wave Reflection in Transonic Test Sections - Part III: Characteristics of Perforated Test-Section Walls with Differential Resistance to Cross-Flow." AEDC-TN-55-44, (AD84158), March 1956.
8. Goethert, B. H. "Physical Aspects of Three-Dimensional Wave Reflections in Transonic Wind Tunnels at Mach Number 1.20 (Perforated, Slotted, and Combined Slotted-Perforated Walls)." AEDC-TR-55-45 (AD84159), March 1956.
9. DuBose, H. C. "Experimental and Theoretical Studies on Three-Dimensional Wave Reflection in Transonic Test Sections - Part II: Theoretical Investigation of the Supersonic Flow Field about a Two-Dimensional Body and Several Three-Dimensional Bodies at Zero Angle of Attack." AEDC-TN-55-43 (AD83539), March 1956.
10. Estabrooks, B. B. "Wall Interference Effects on Axisymmetric Bodies in Transonic Wind Tunnels with Perforated Wall Test Section." AEDC-TR-59-12, (AD216698), June 1959.

11. Pindzola, M. and Chew, W. L. "A Summary of Perforated Wall Wind Tunnel Studies at the Arnold Engineering Development Center." AEDC-TR-60-9 (AD241573), August 1960.
12. Chew, W. L., Jr. "Determination of Optimum Operating Parameters for the 1-Foot Transonic Tunnel Utilizing Cone-Cylinder Bodies of Revolution," AEDC-TN-60-69 (AD235384), April 1960.
13. Binion, T. W., Jr. "An Investigation of Three-Dimensional Wall Interference in a Variable Porosity Transonic Wind Tunnel." AEDC-TR-74-76 (AD787658), October 1974.
14. Hsieh, T. "Hemisphere-Cylinder in Transonic Flow, $M_{\infty} = 0.7 \sim 1.0$." *AIAA Journal*, Vol. 13, No. 10, October 1975, pp. 1411-1413.

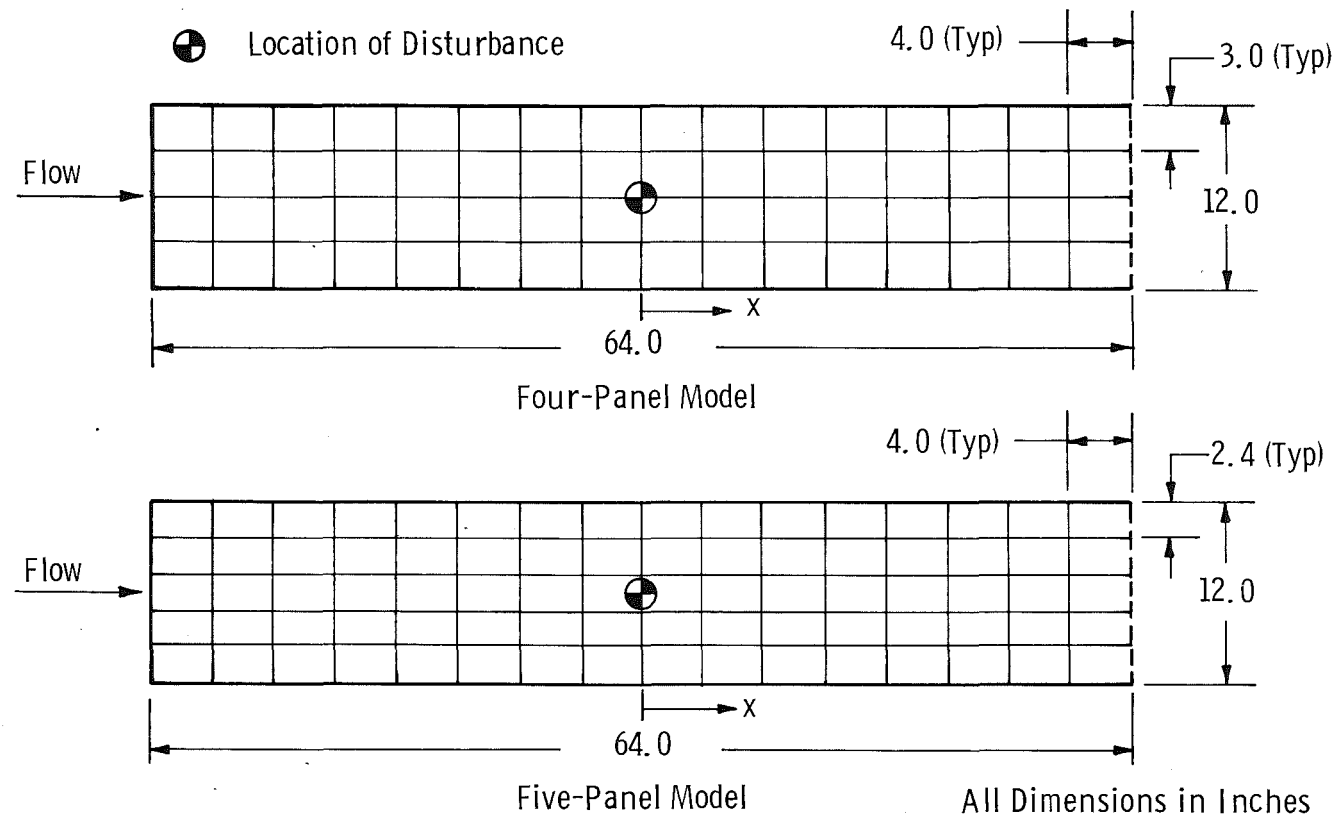


Figure 1. Vortex lattice representations of a wind tunnel sidewall.

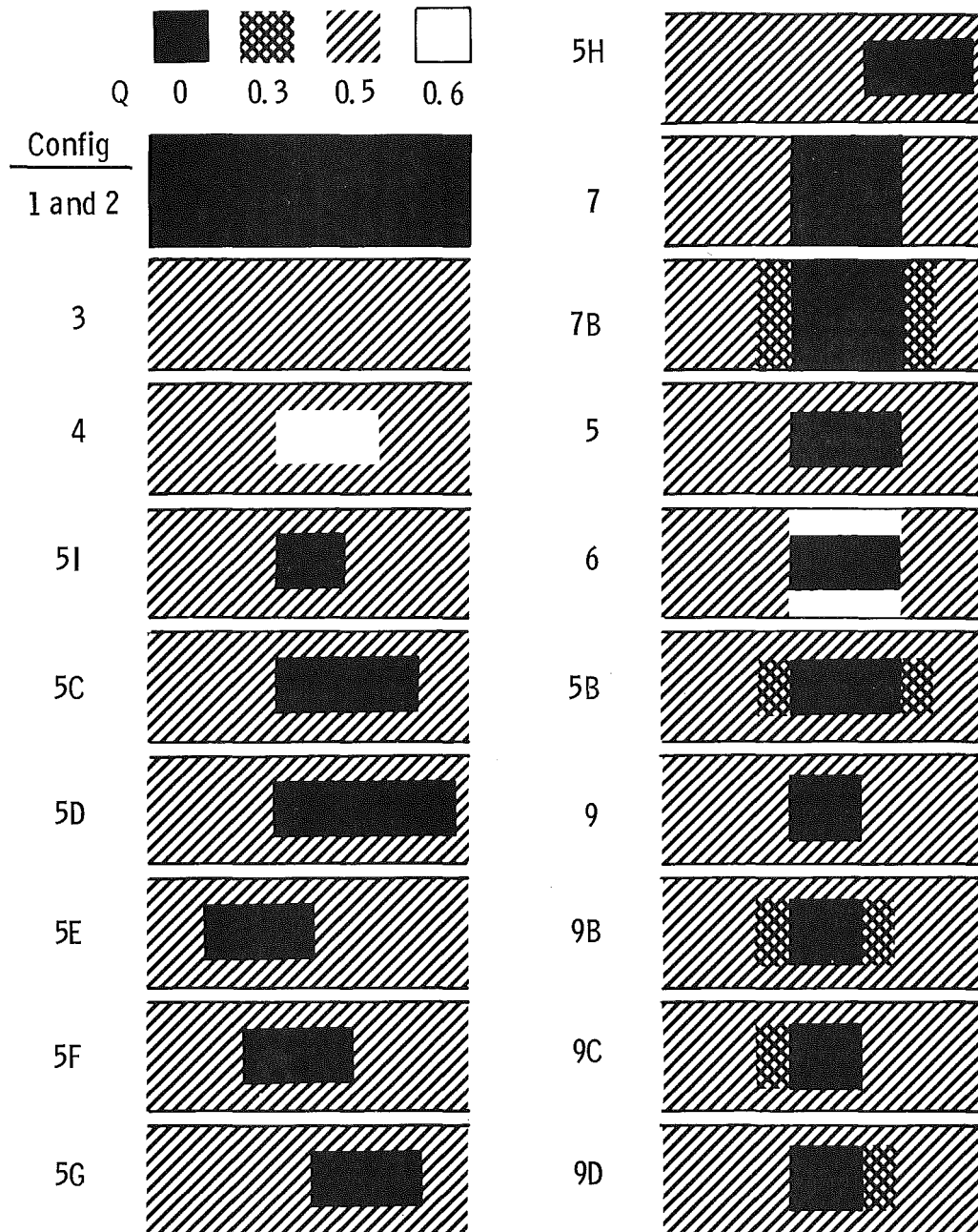
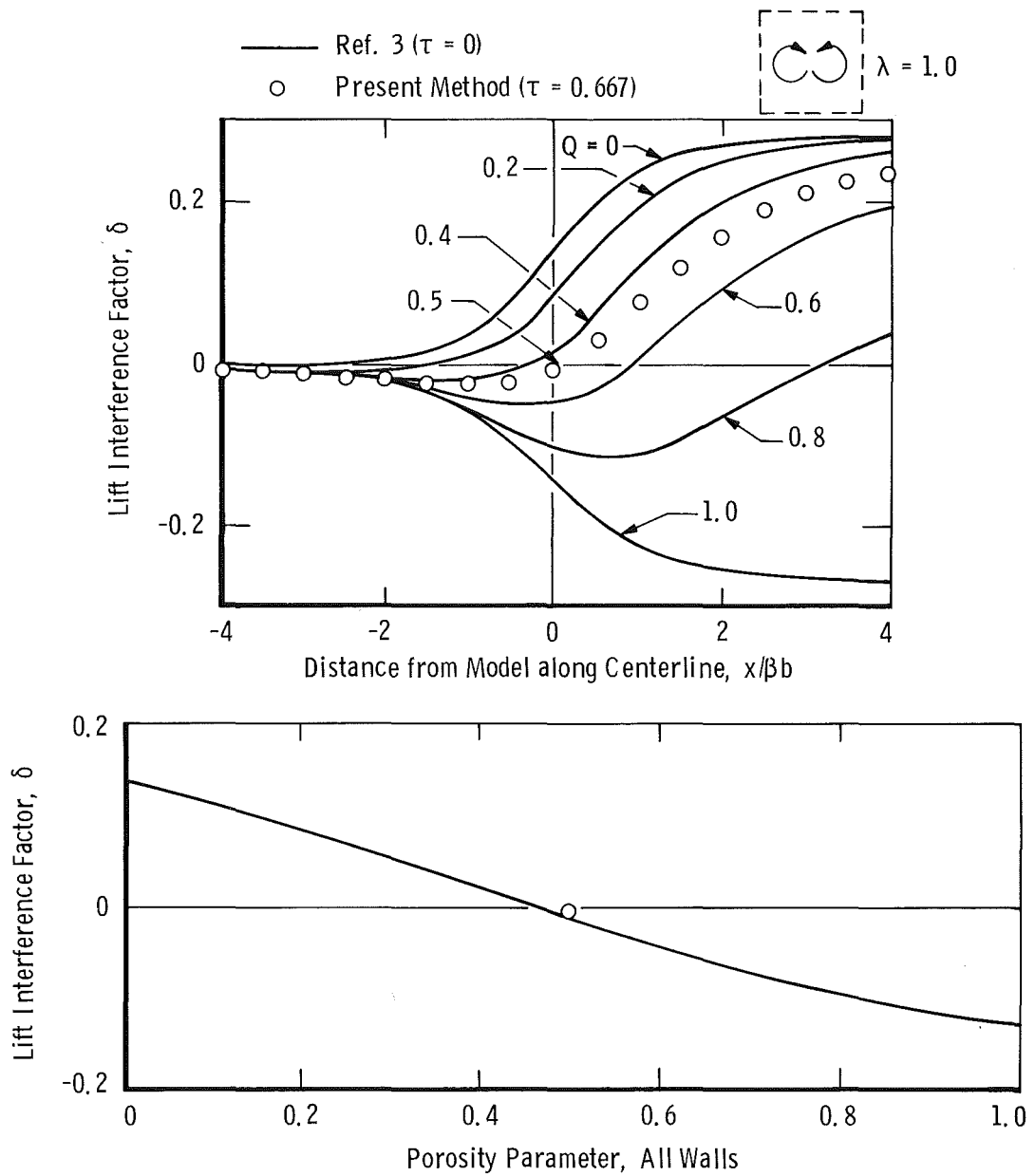
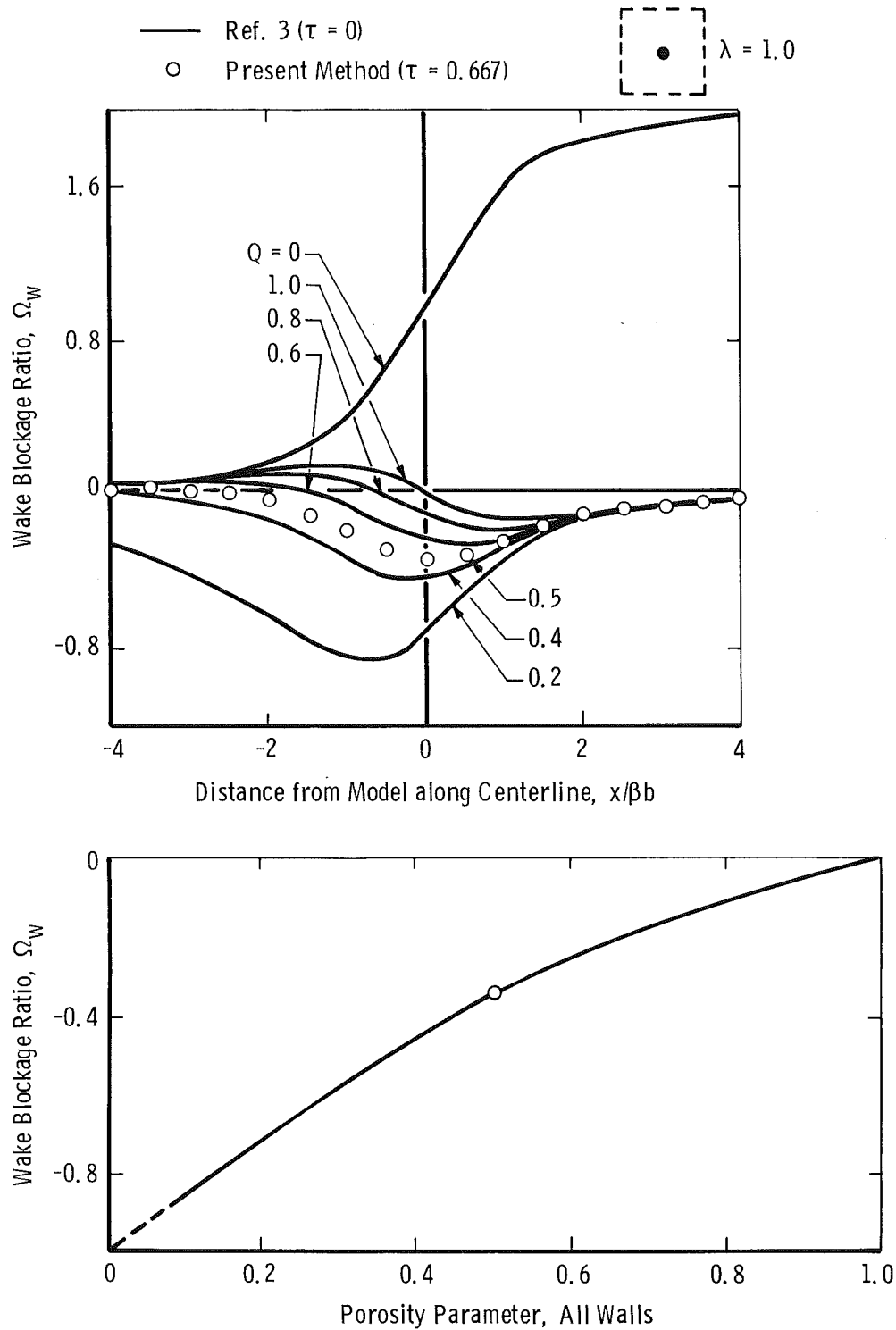


Figure 2. Sidewall configurations for analytical study.

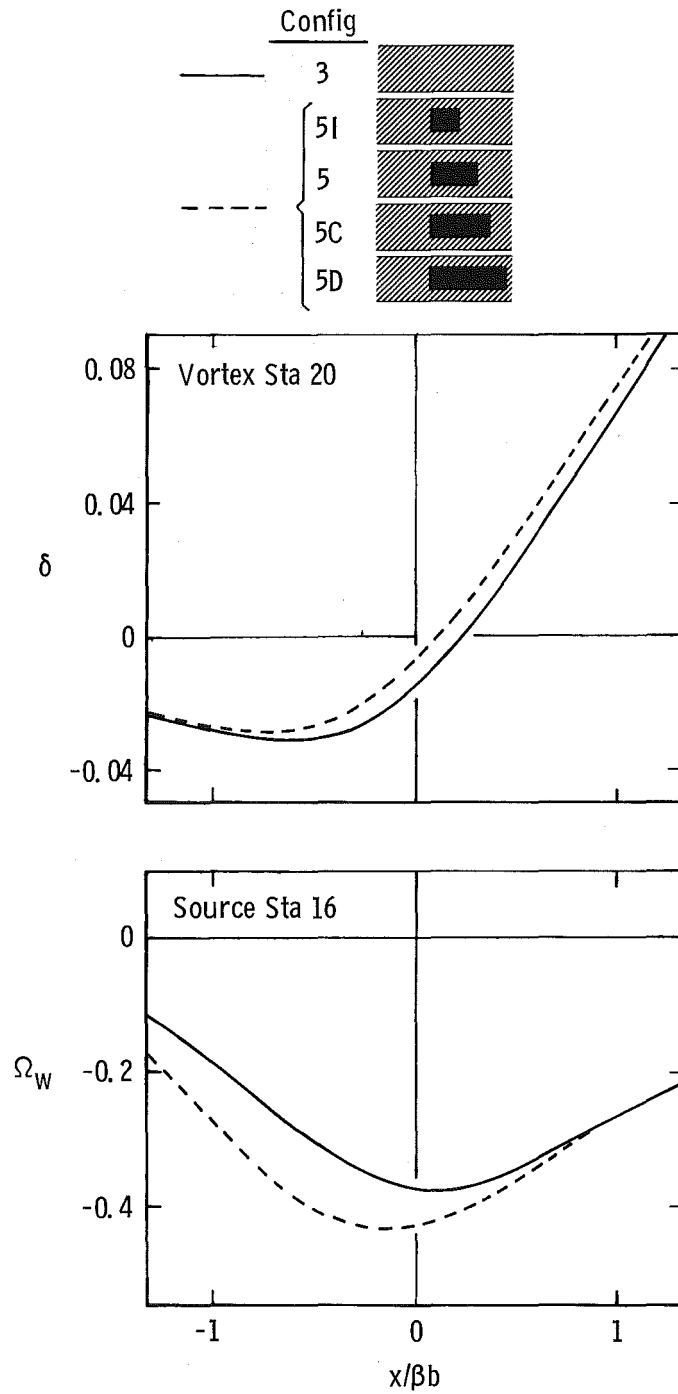


a. Lift interference

Figure 3. Comparison of present method and point-matching technique (Ref. 3).

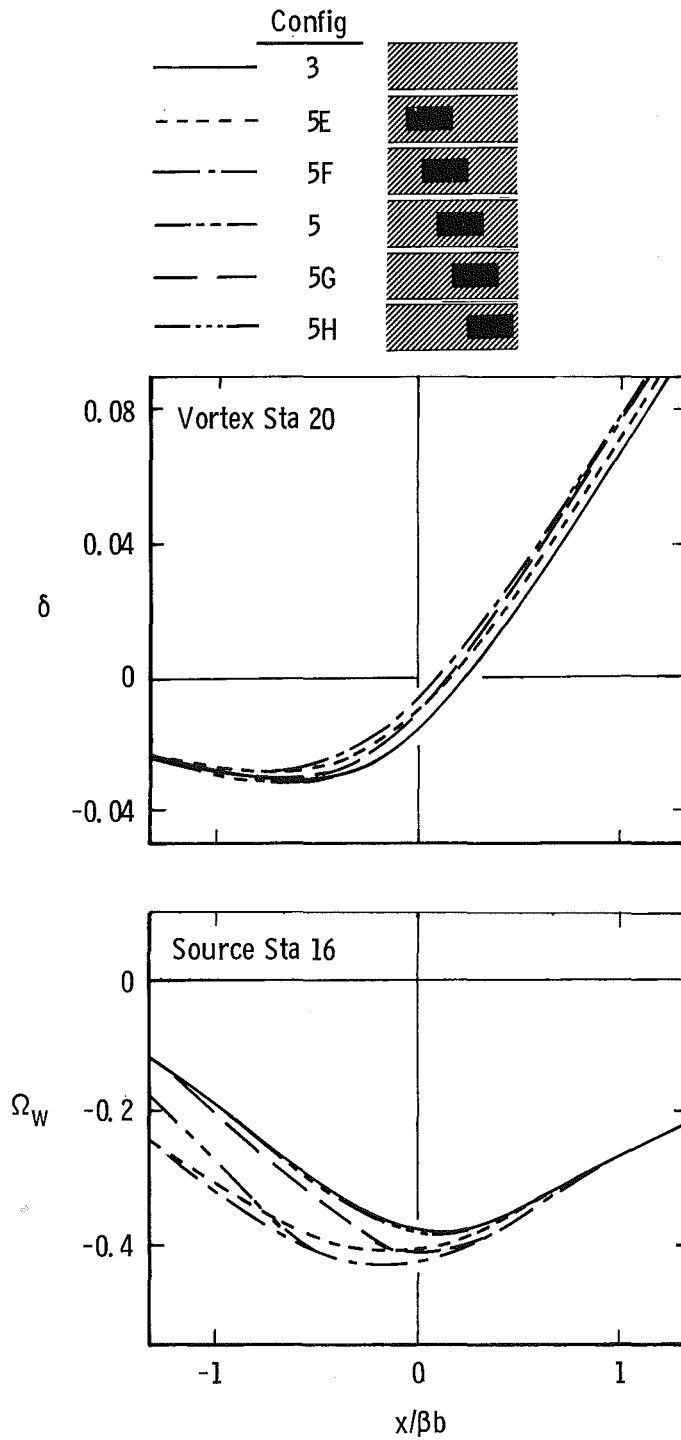


b. Wake blockage
 Figure 3. Concluded.

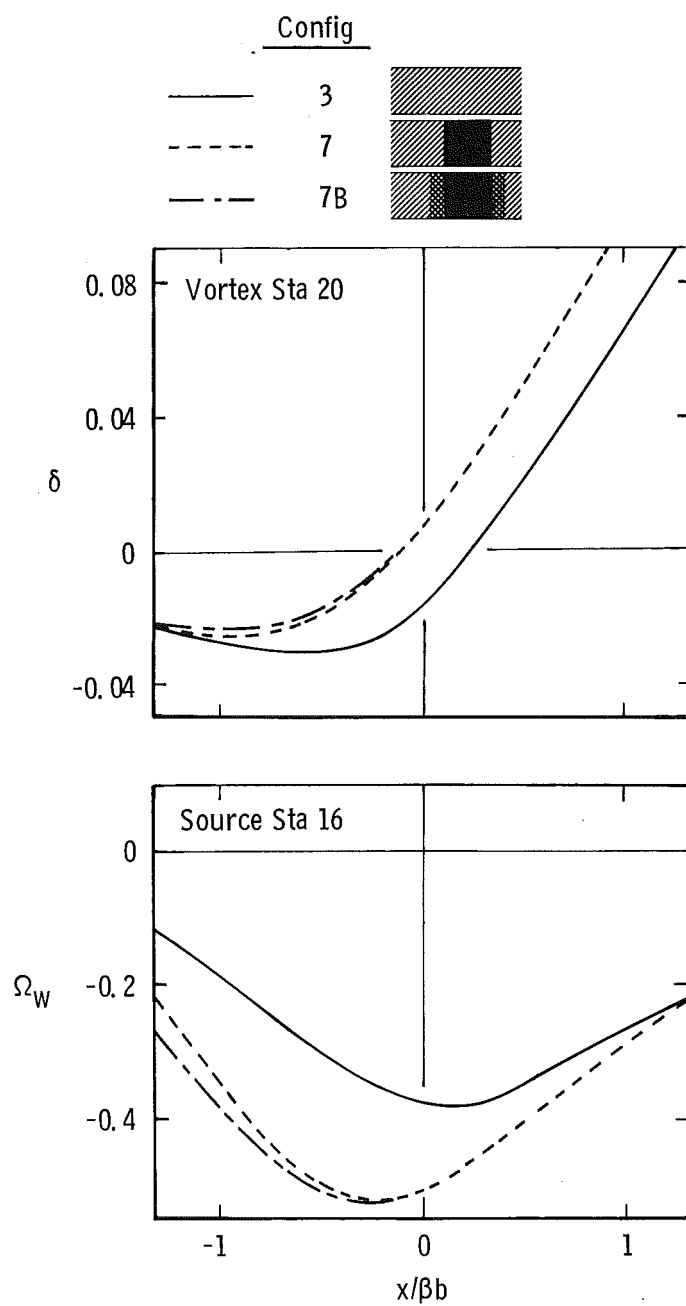


a. Effect of window length
(leading edge fixed)

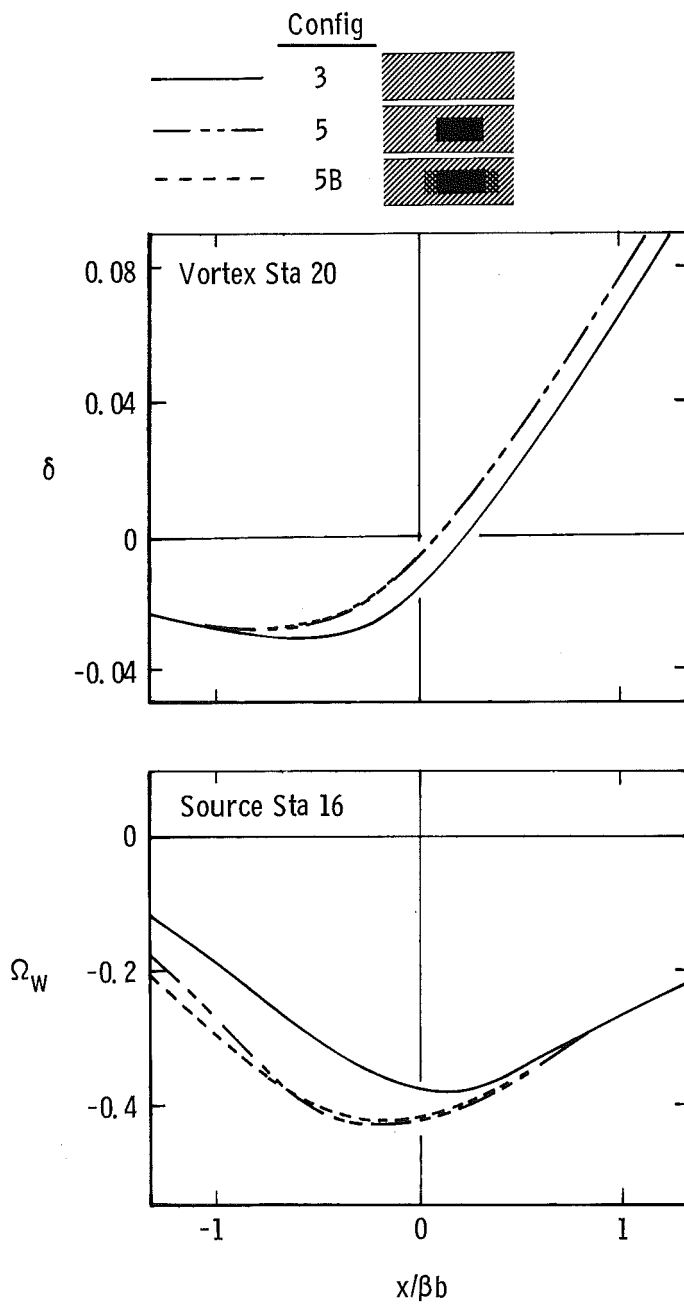
Figure 4. Distribution of lift interference factor and wake blockage ratio along wind tunnel centerline for several wall configurations.



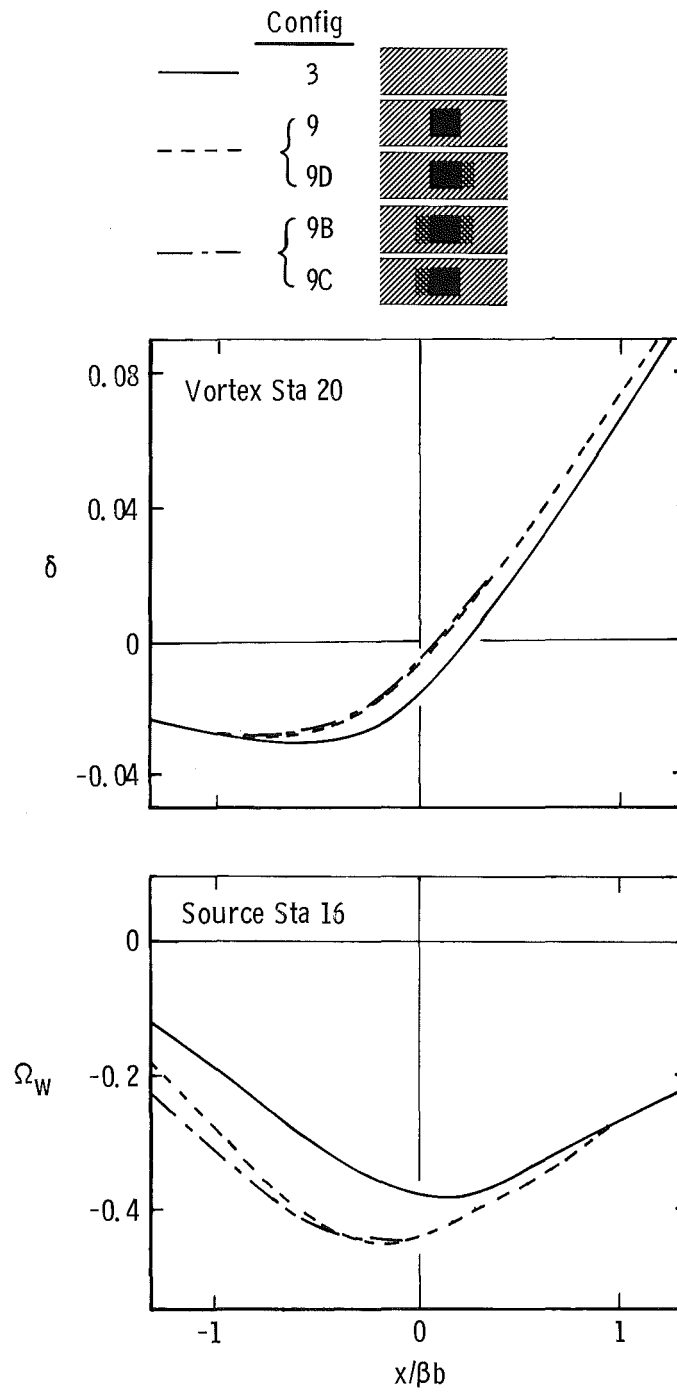
b. Effect of window position
(constant length)
Figure 4. Continued.



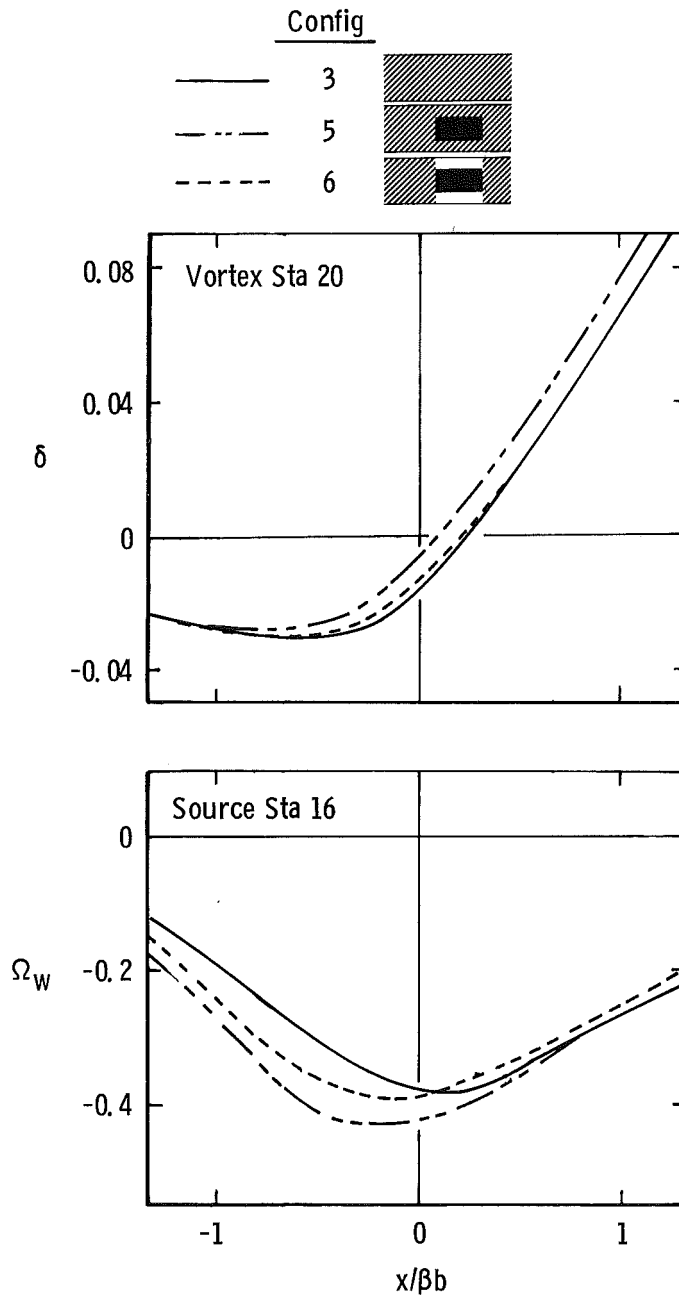
c. Effect of transition regions
(large window)
Figure 4. Continued.



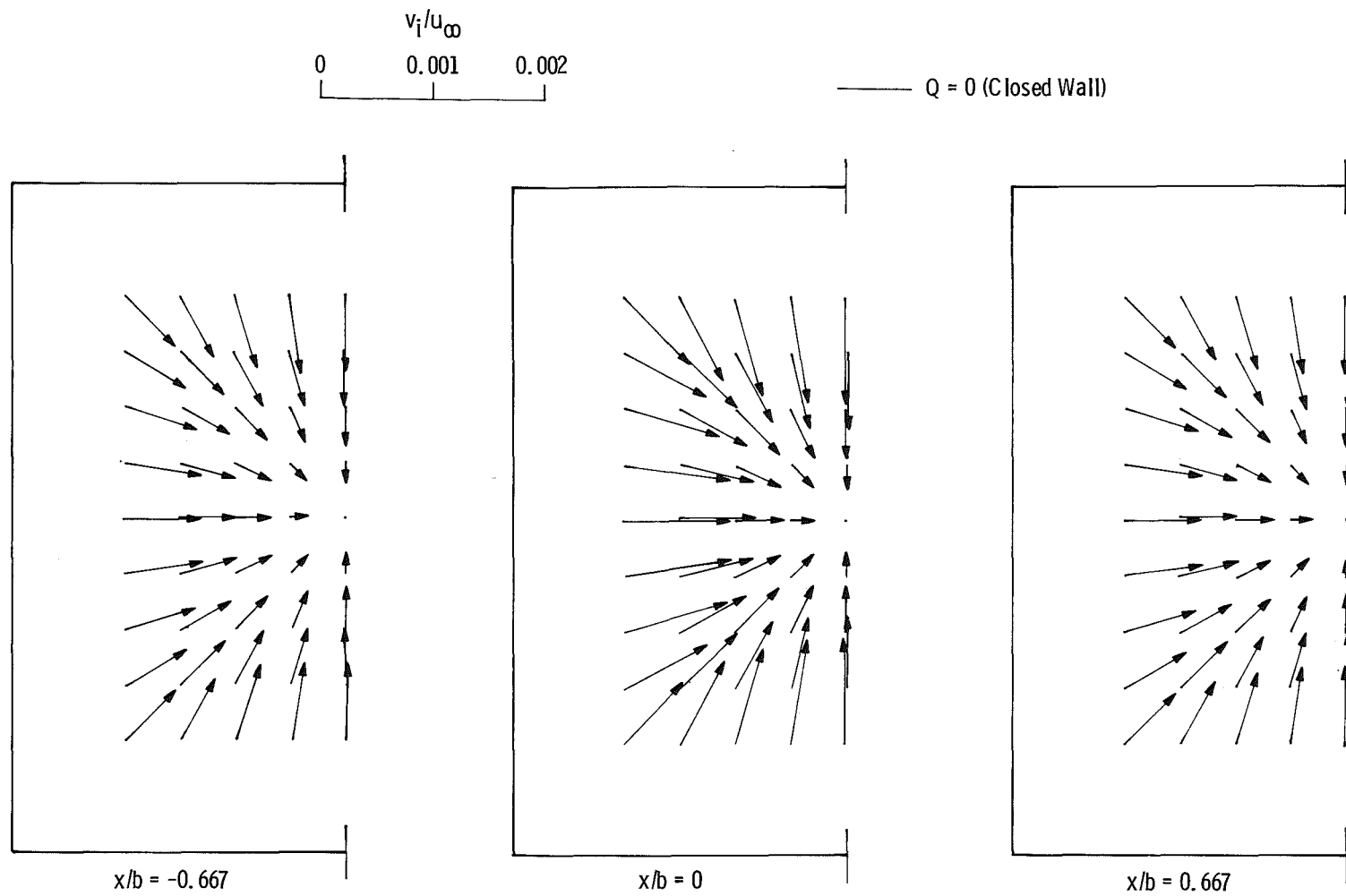
d. Effect of transition regions
(medium windows)
Figure 4. Continued.



e. Effect of transition regions
(small window)
Figure 4. Continued.

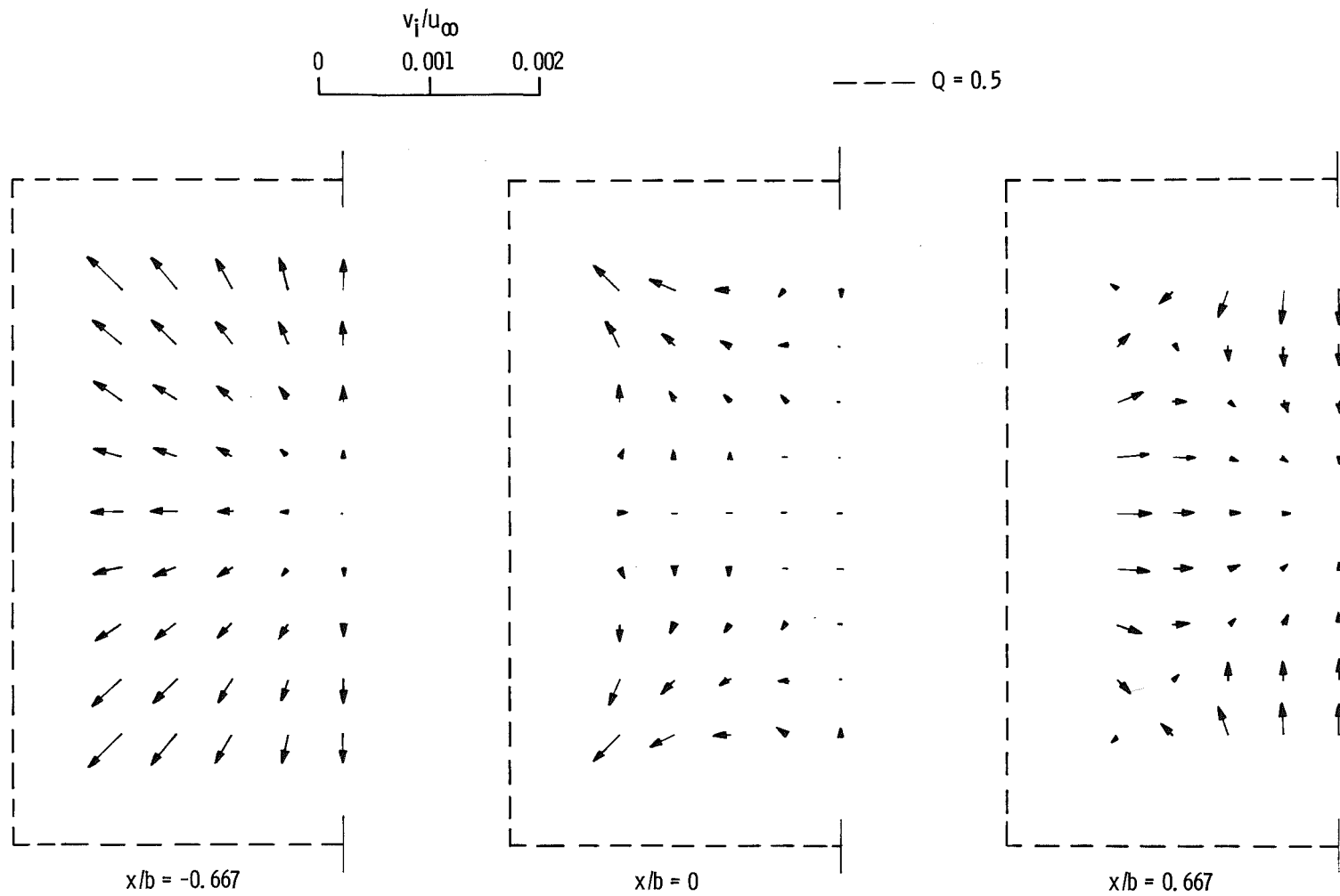


f. Effect of constant average porosity
Figure 4. Concluded.

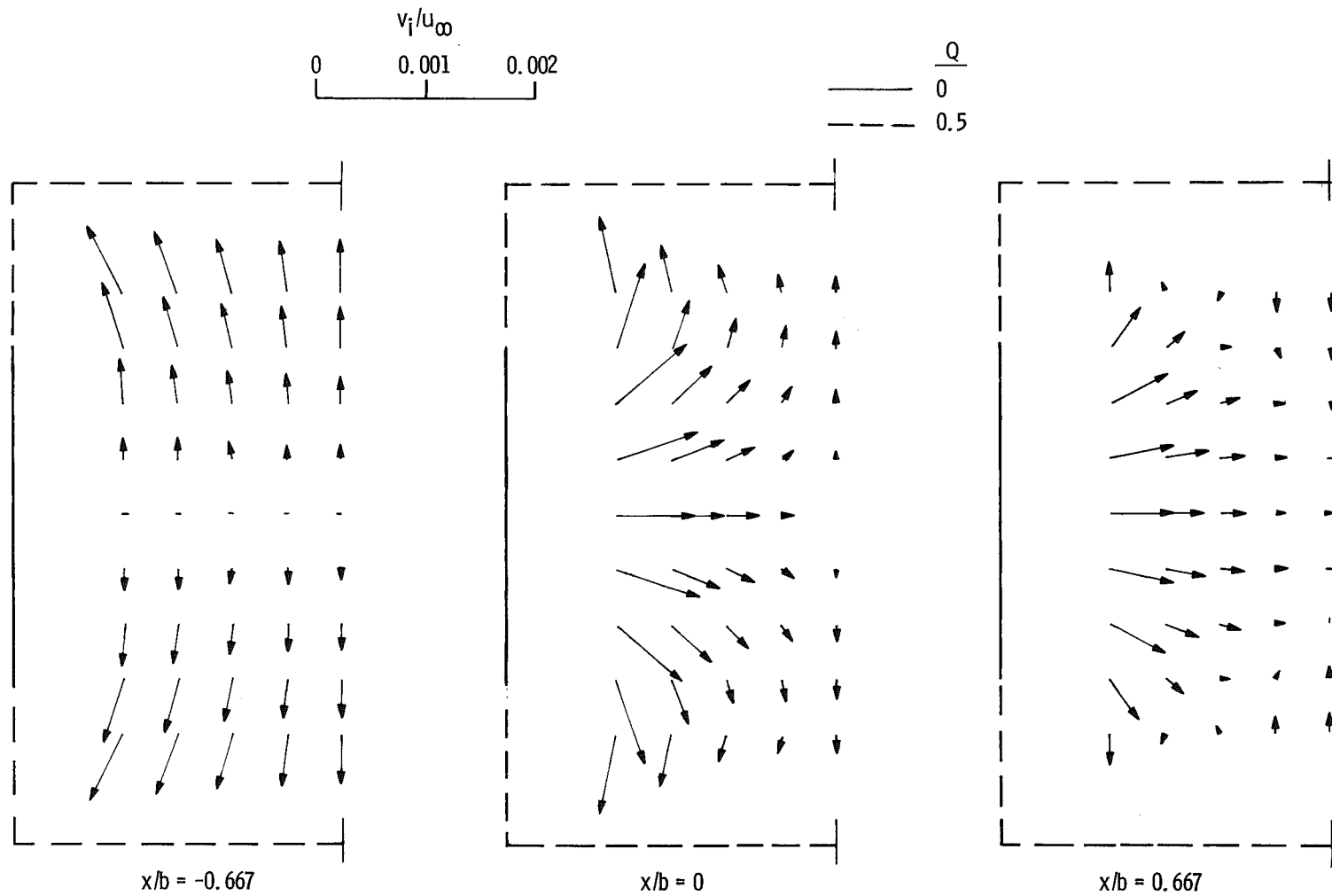


a. Configuration 1 (all walls closed)

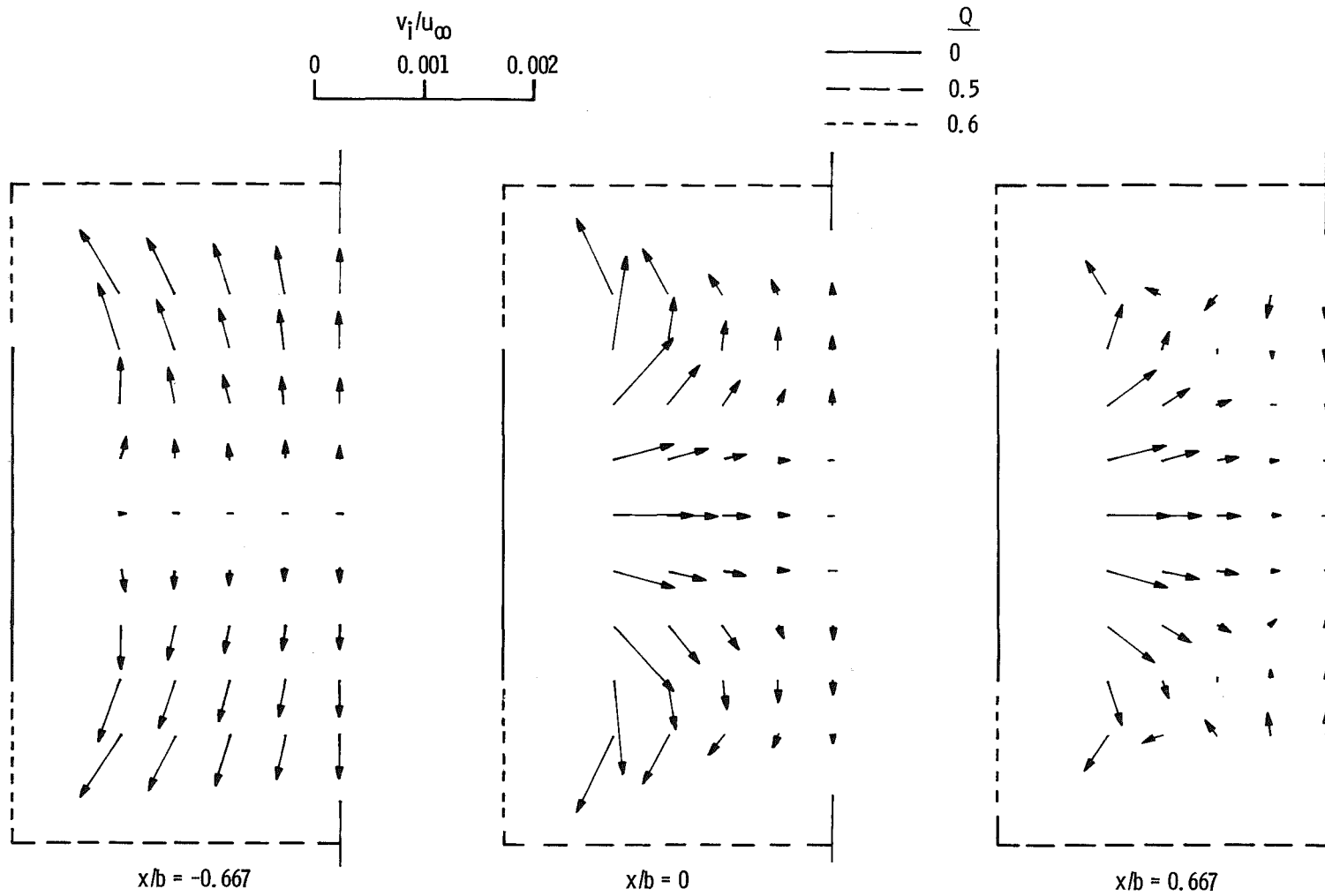
Figure 5. Interference velocity vector projections on constant x -planes resulting from a unit source (wake blockage disturbance) at $x = 0$.



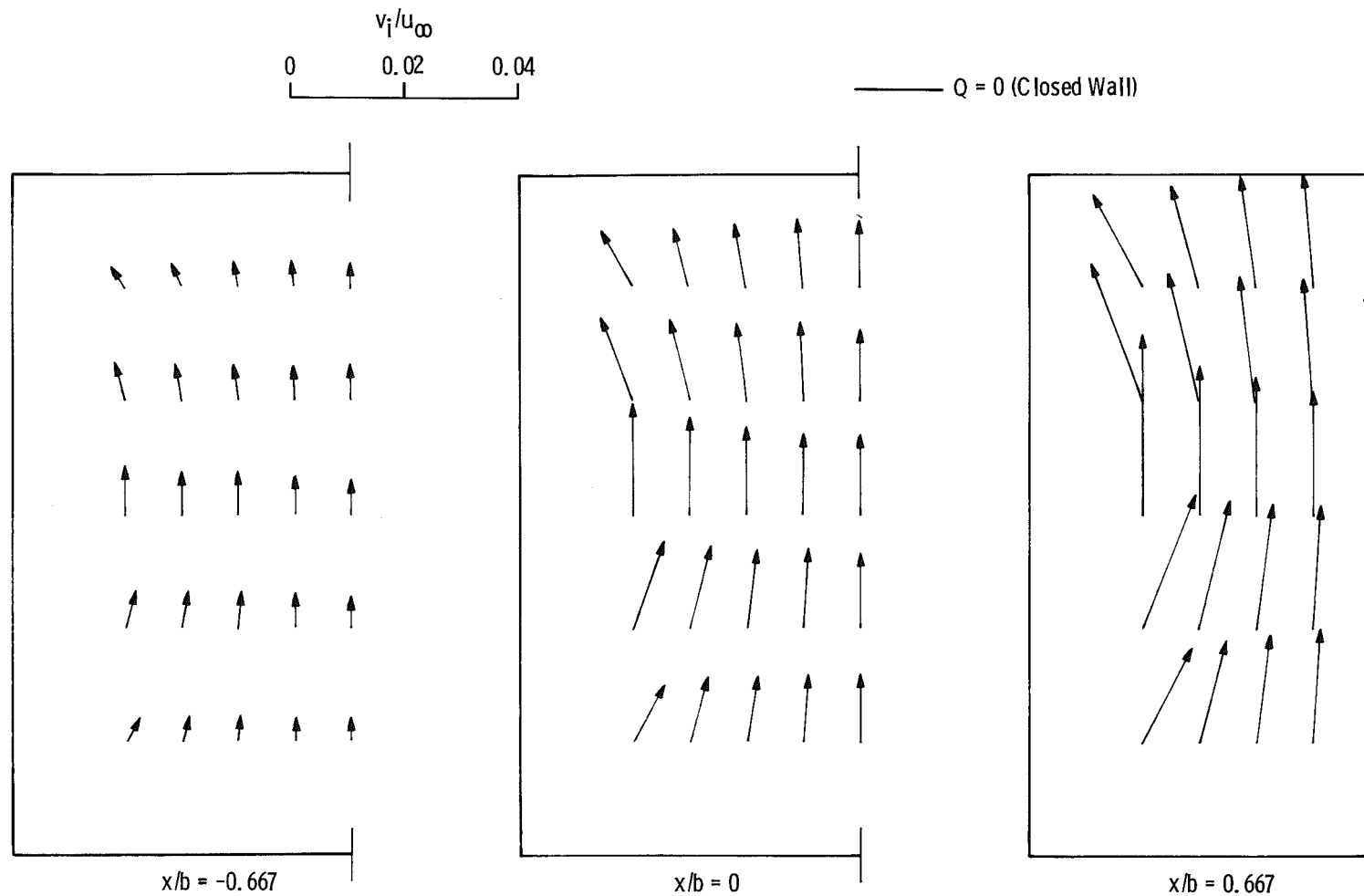
b. Configuration 3
Figure 5. Continued.



c. Configuration 5
Figure 5. Continued.



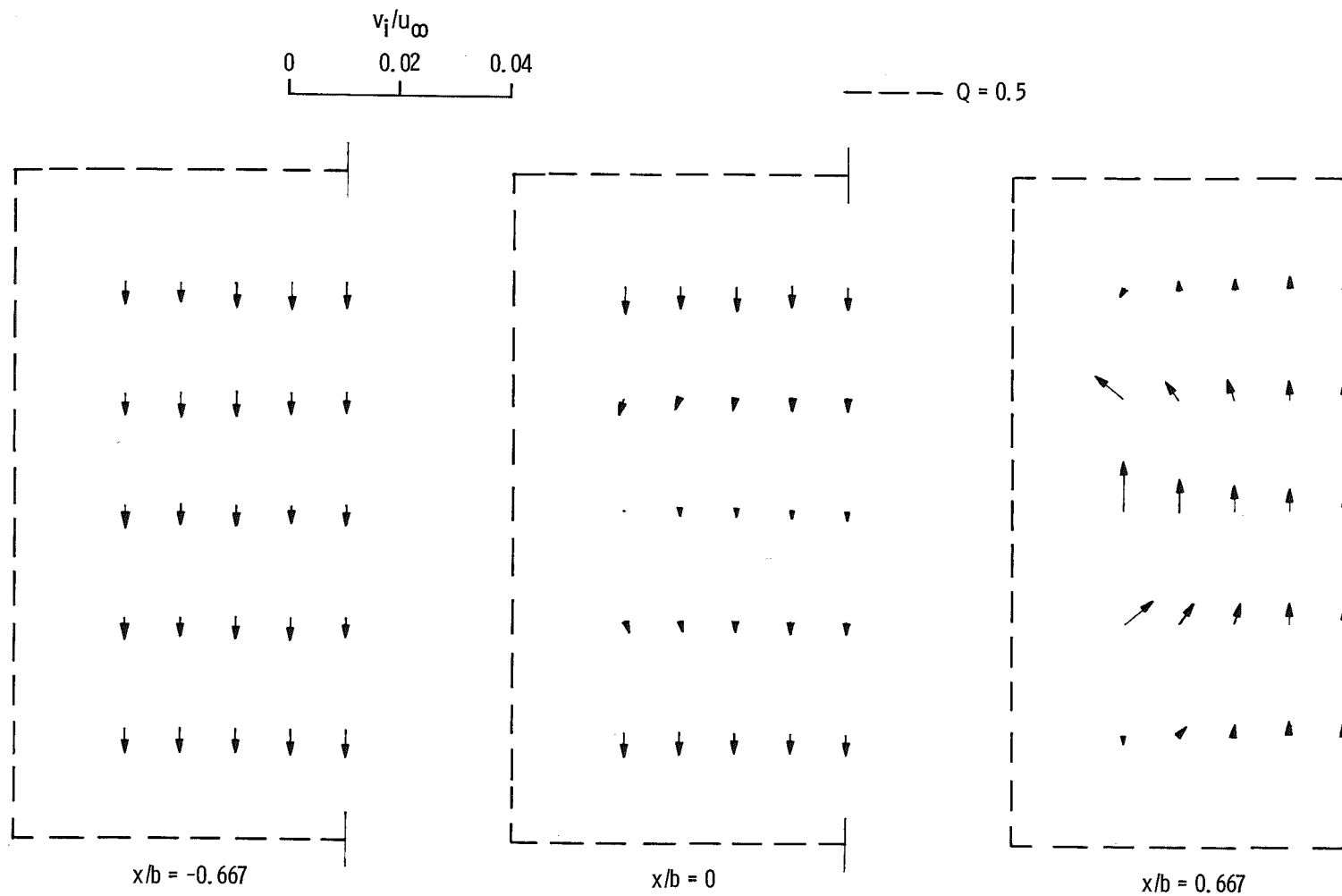
d. Configuration 6
Figure 5. Concluded.



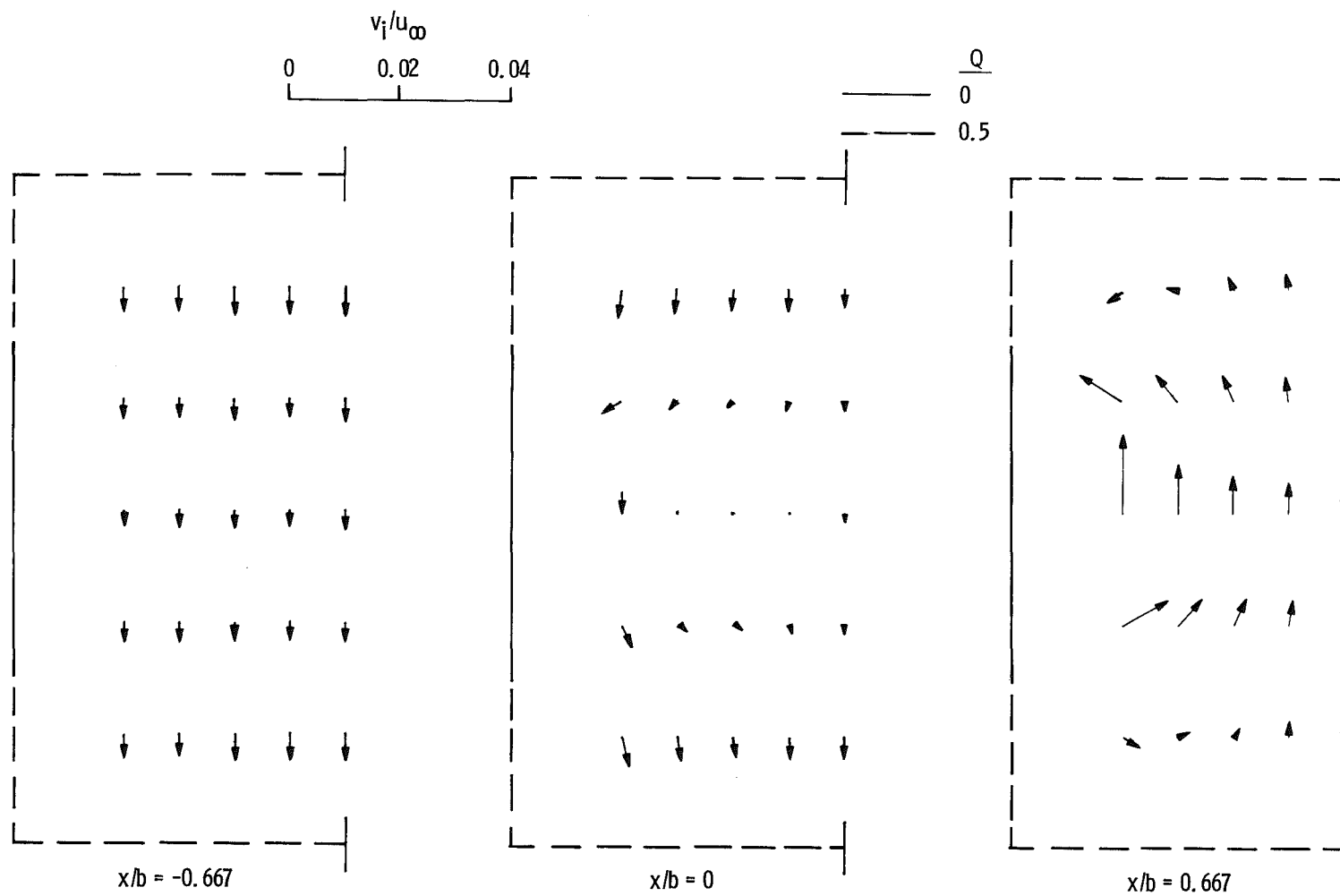
a. Configuration 1 (all walls closed)

Figure 6. Interference velocity vector projections on constant x -planes resulting from a unit vortex ($\zeta = 0.667$) (lift disturbance) at $x = 0$.

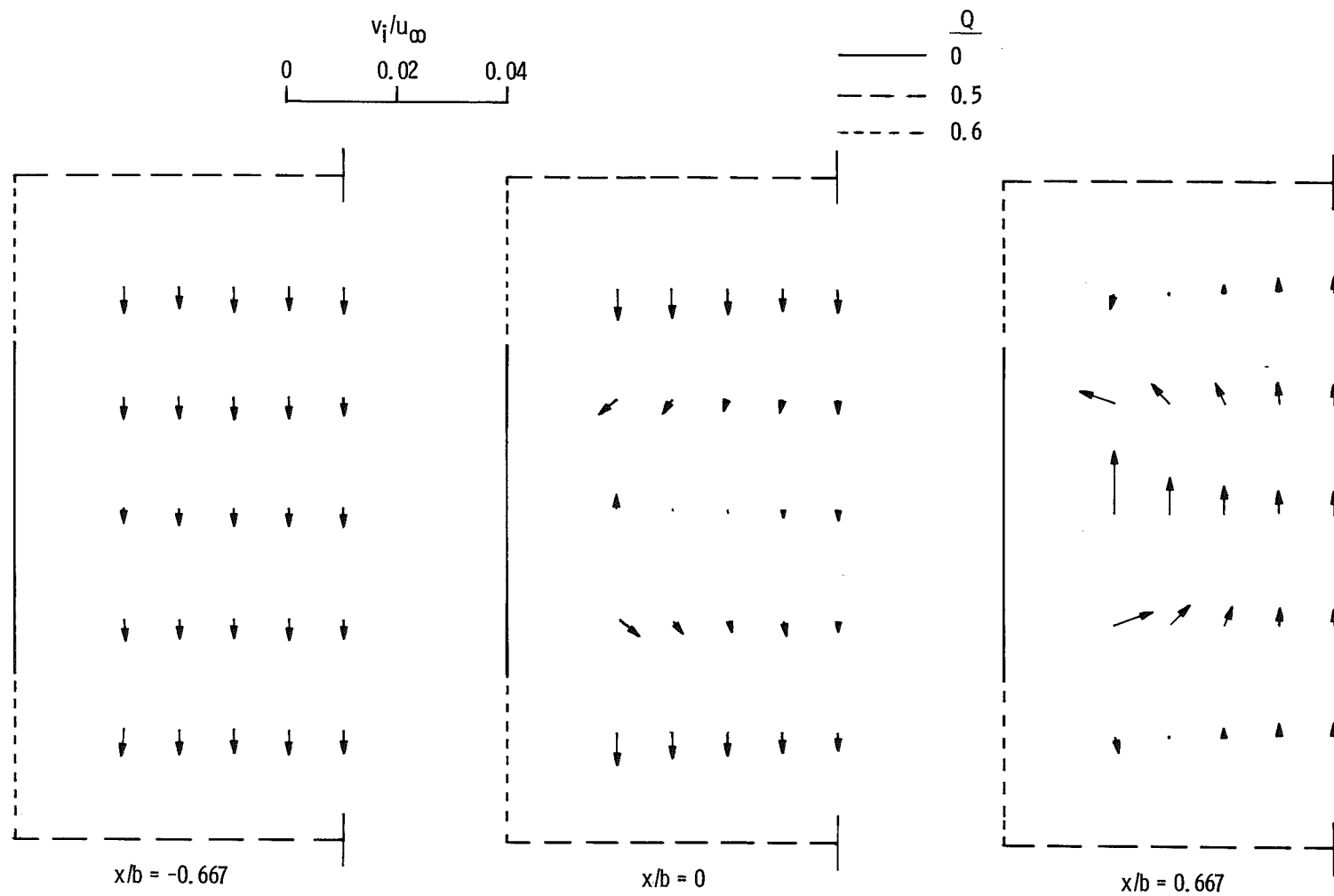
30



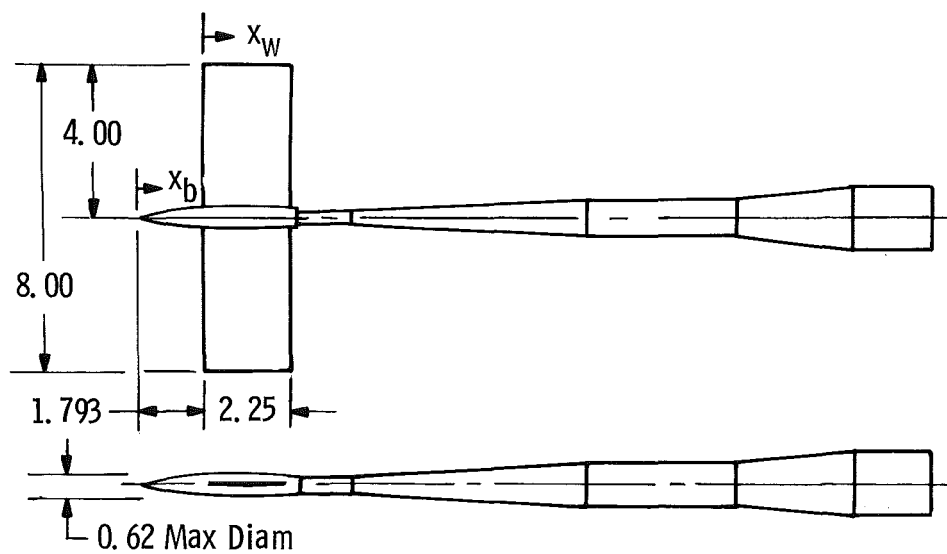
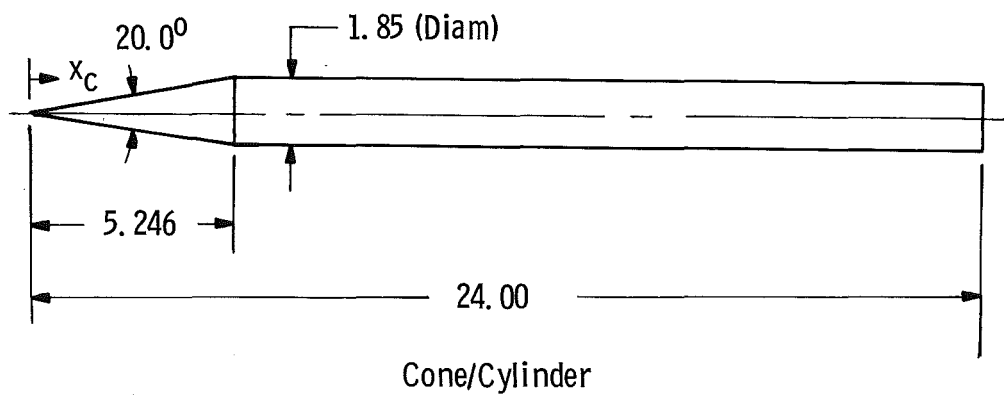
b. Configuration 3
Figure 6. Continued.



c. Configuration 5
Figure 6. Continued.



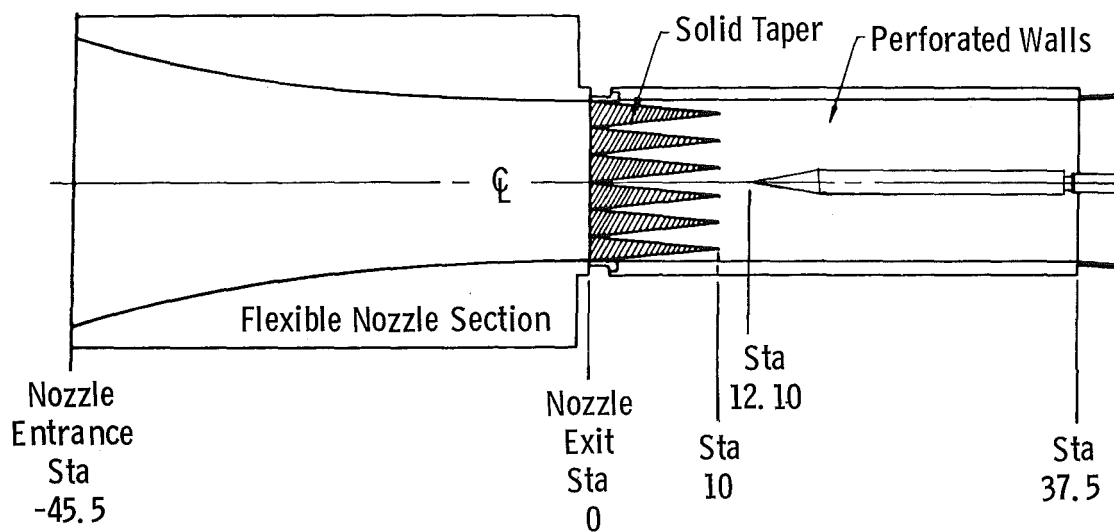
d. Configuration 6
Figure 6. Concluded.



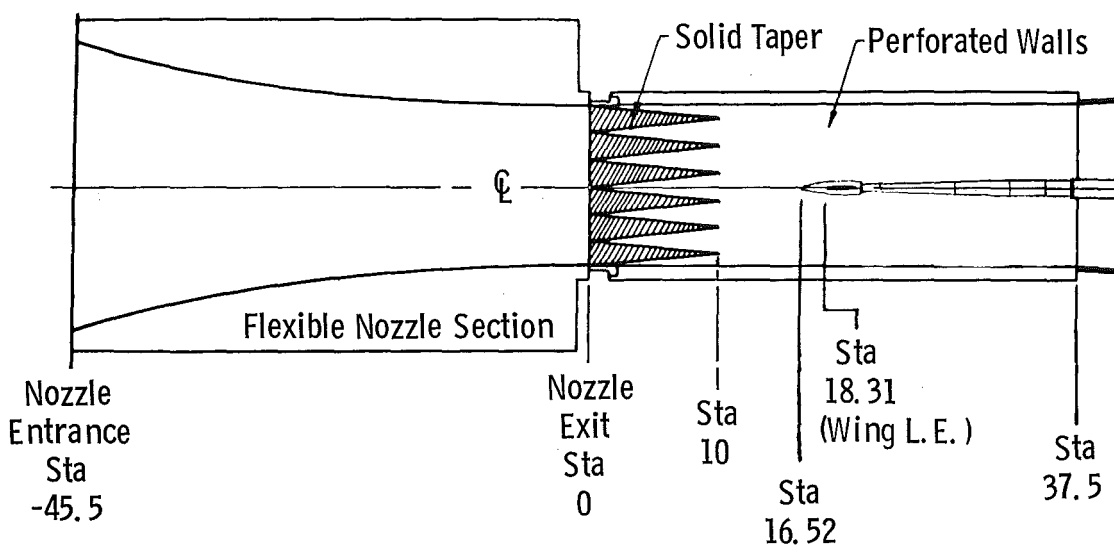
Wing/Centerbody

All Dimensions in Inches

Figure 7. Test models.



Cone/Cylinder



Wing/Centerbody

Figure 8. Installation in Tunnel 1T.

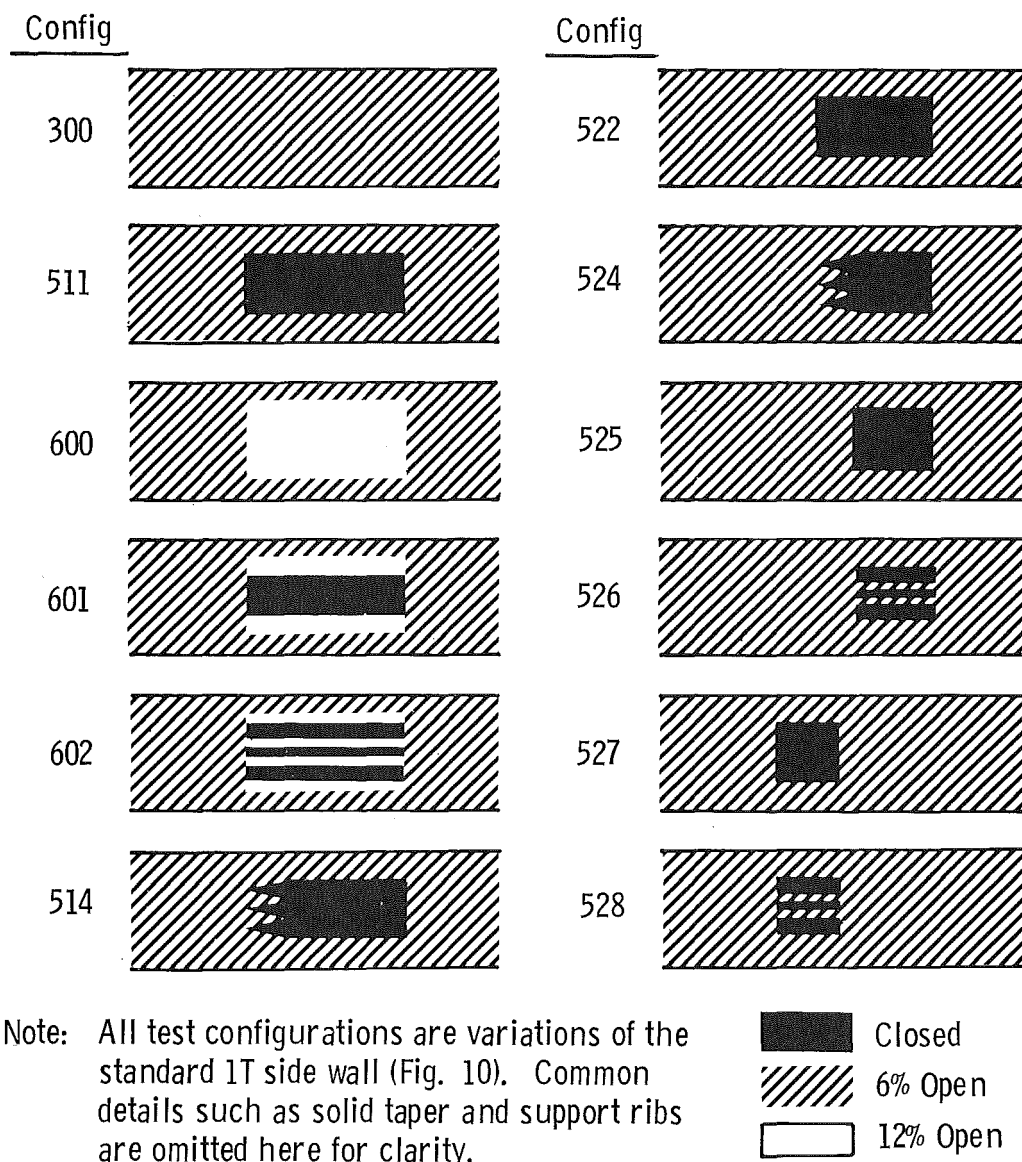


Figure 9. Sidewall configurations tested.

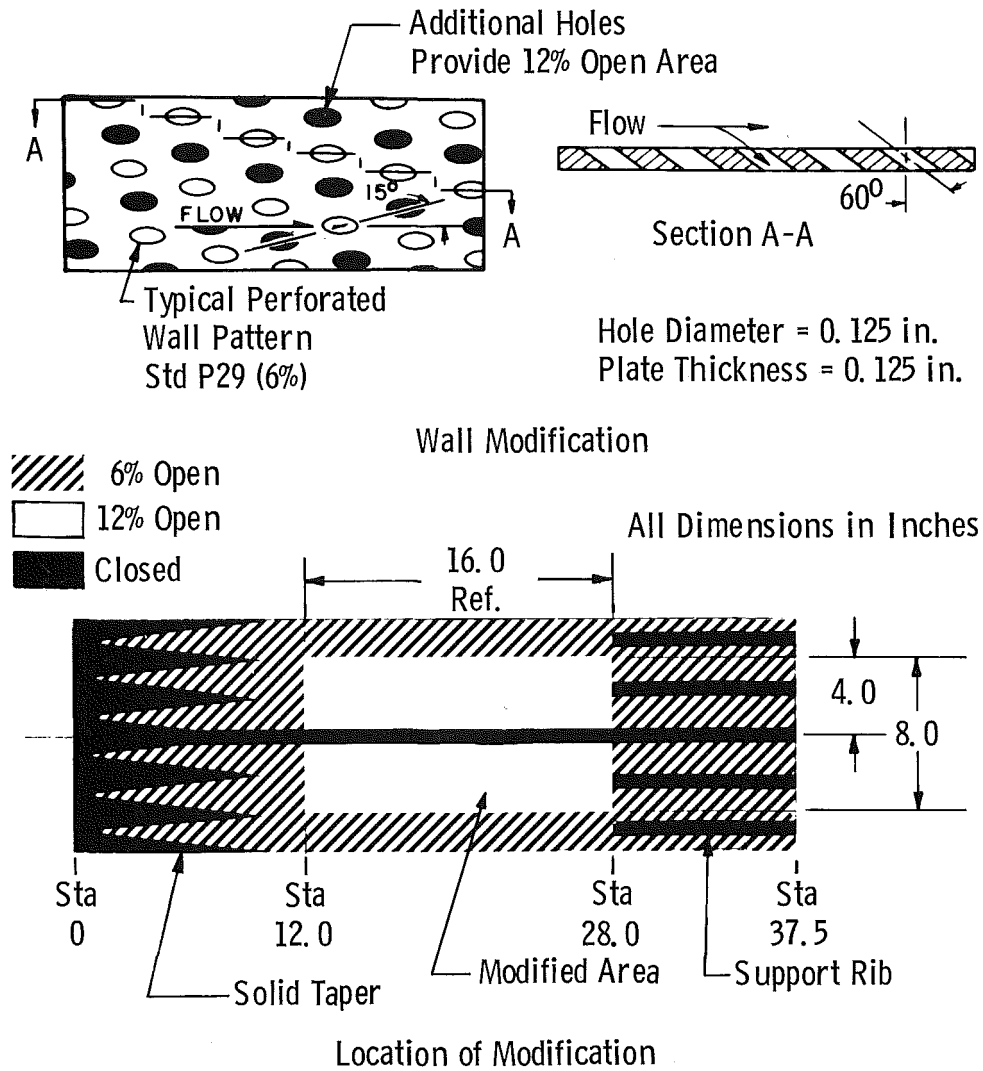


Figure 10. Modification of Tunnel 1T standard sidewalls.

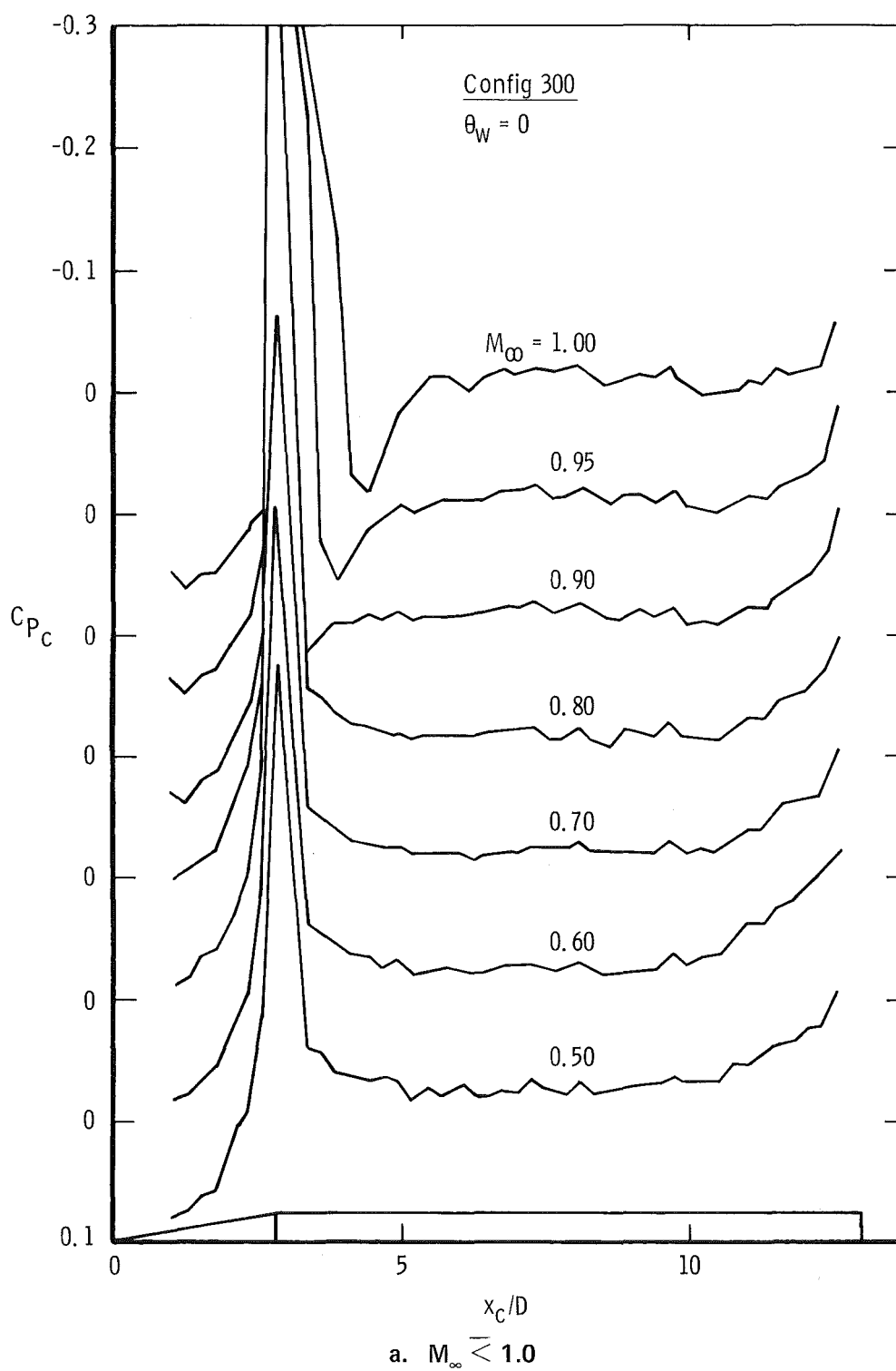
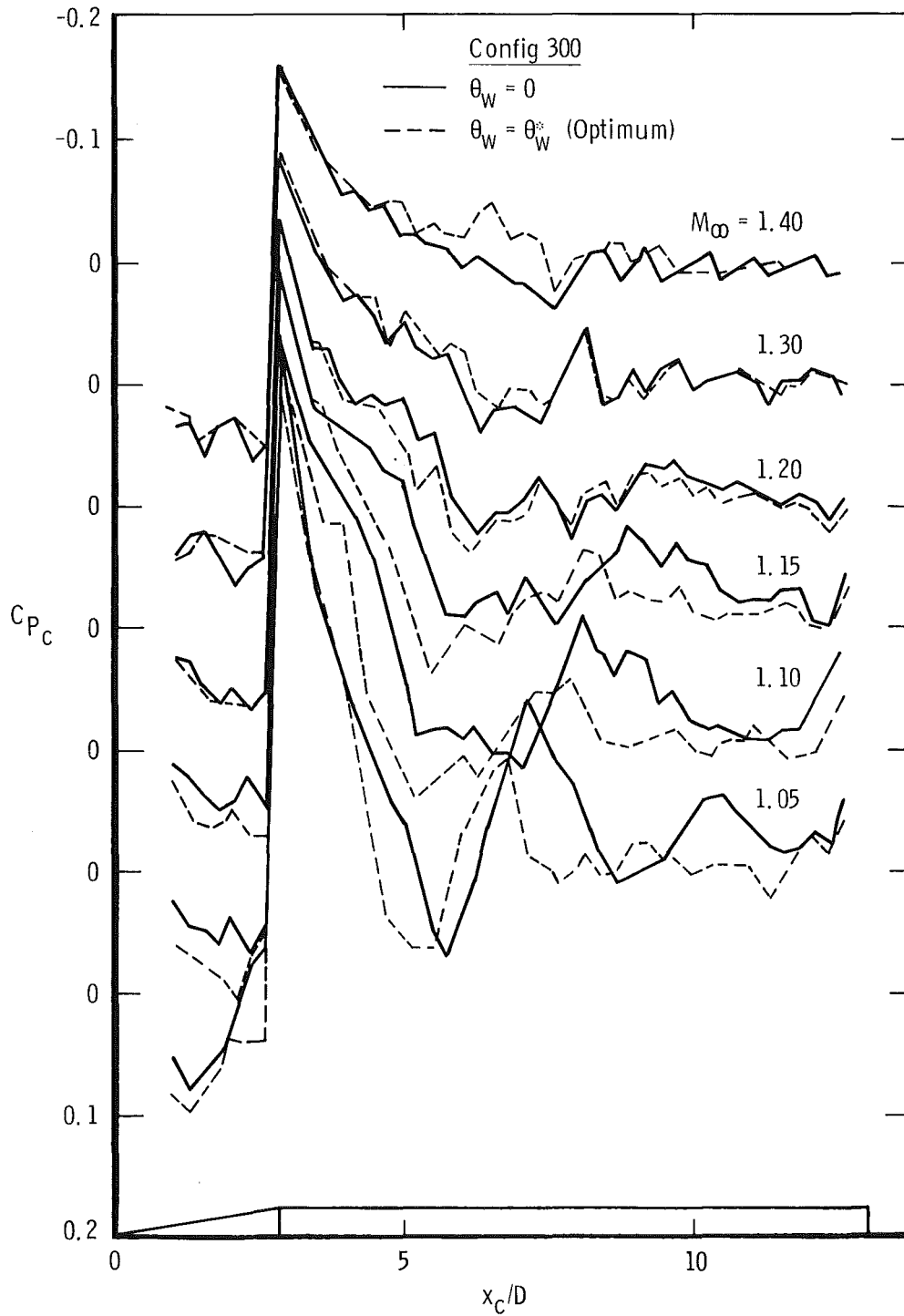
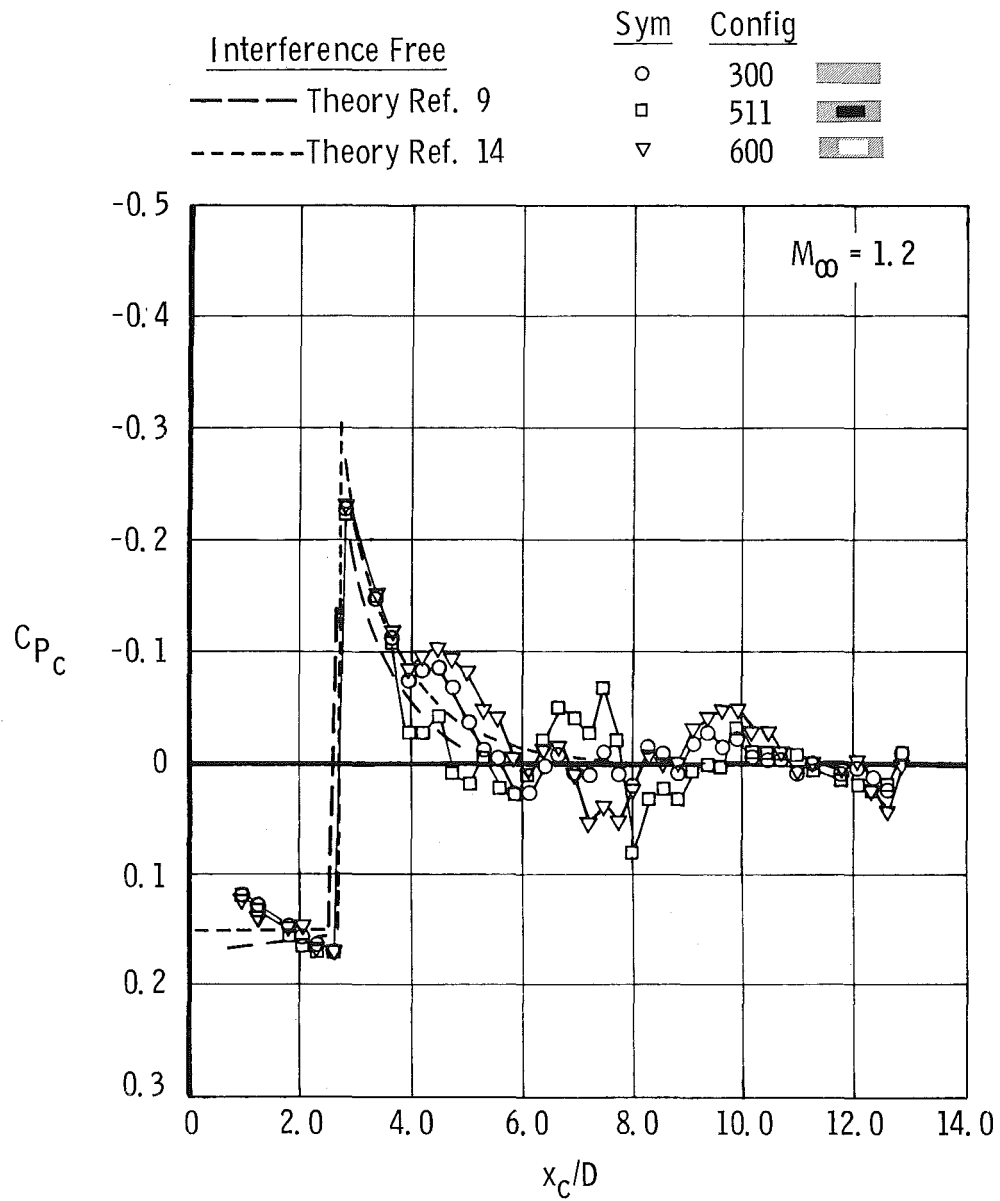


Figure 11. Axial distribution of pressure coefficient on cone/cylinder for configuration 300 and Mach numbers from 0.5 through 1.4.

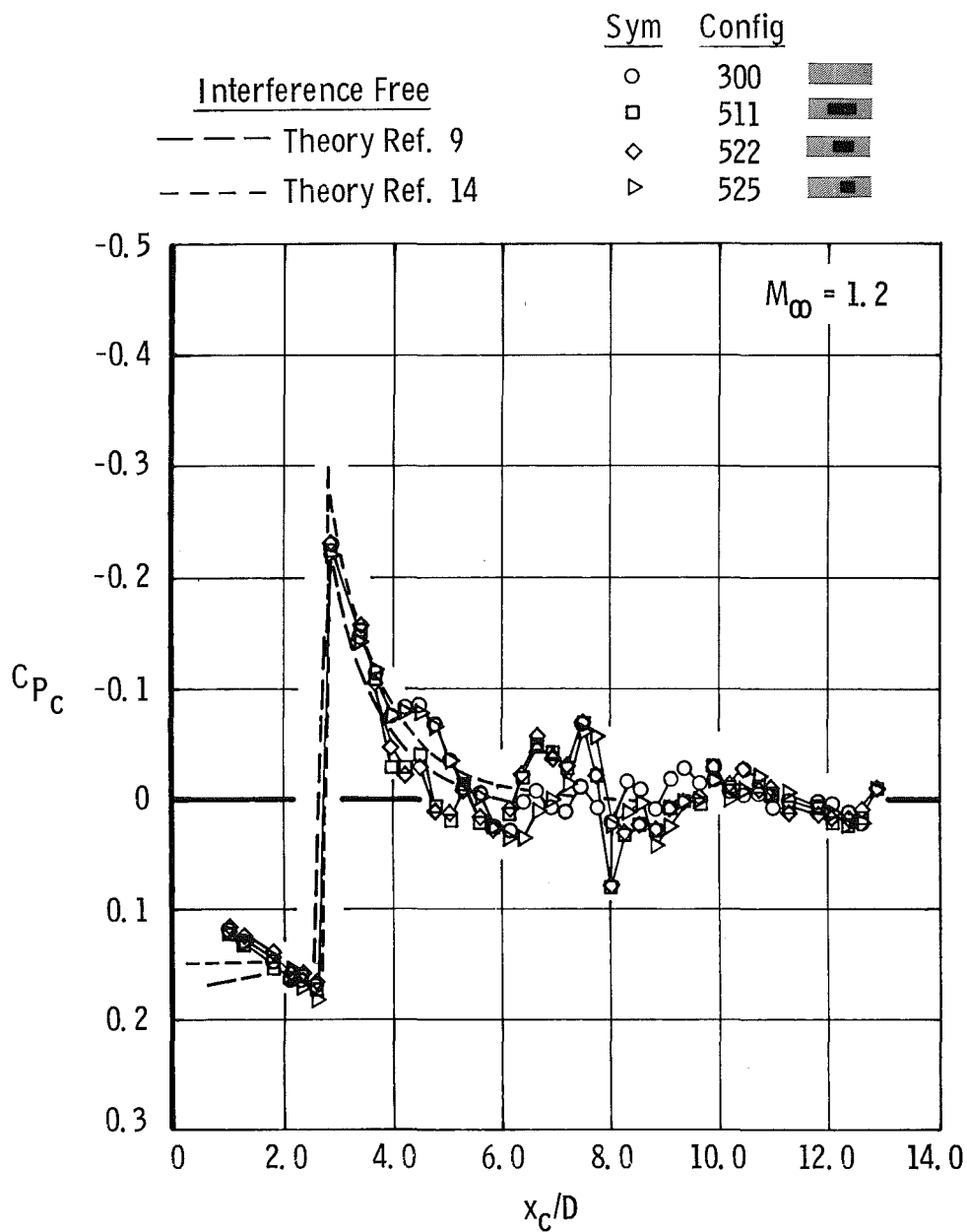


b. $M_\infty > 1.0$
Figure 11. Concluded.



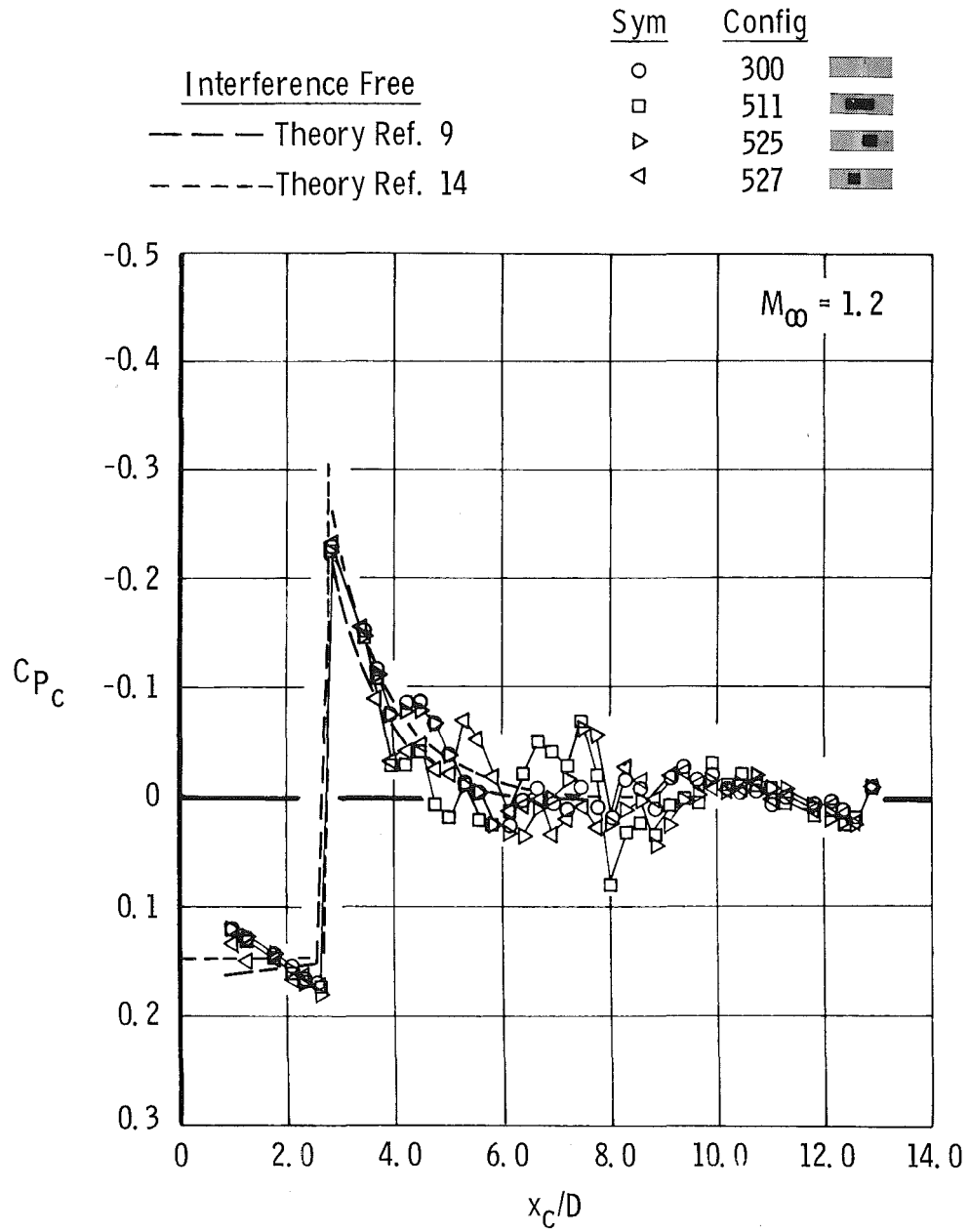
a. Extreme conditions

Figure 12. Axial distribution of pressure coefficient on cone/cylinder for selected wall configurations and Mach numbers.

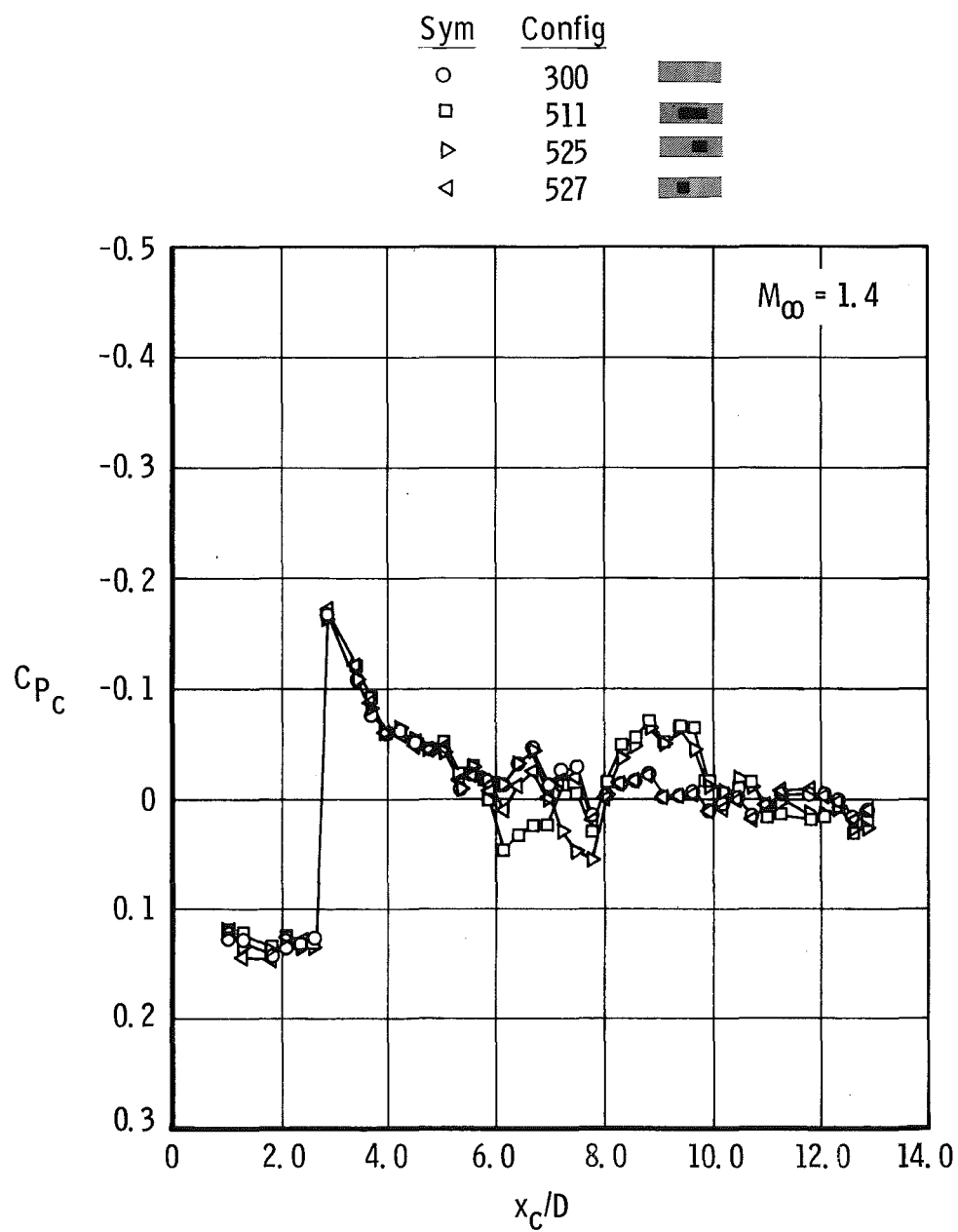


b. Window length (trailing edge fixed)

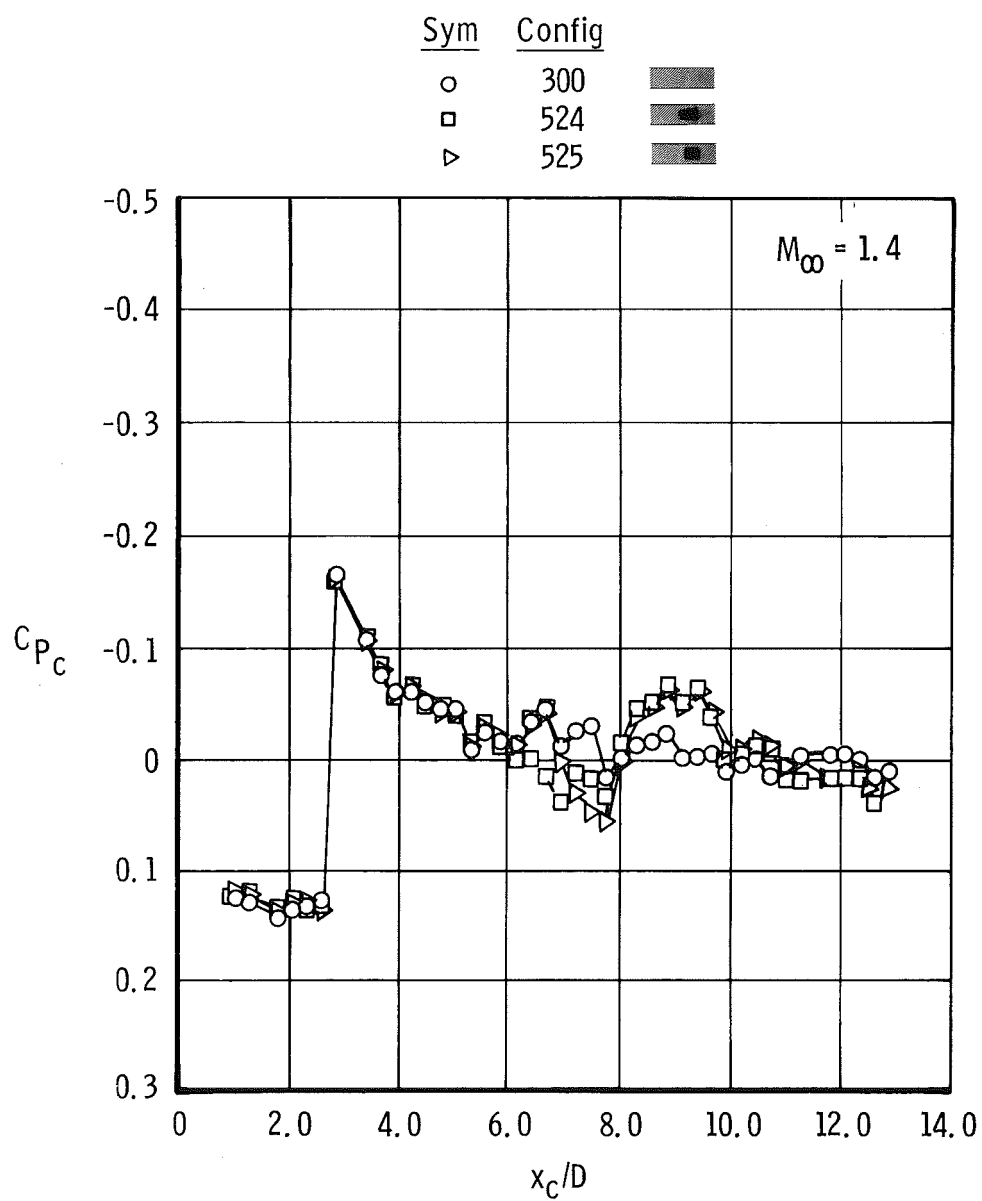
Figure 12. Continued.



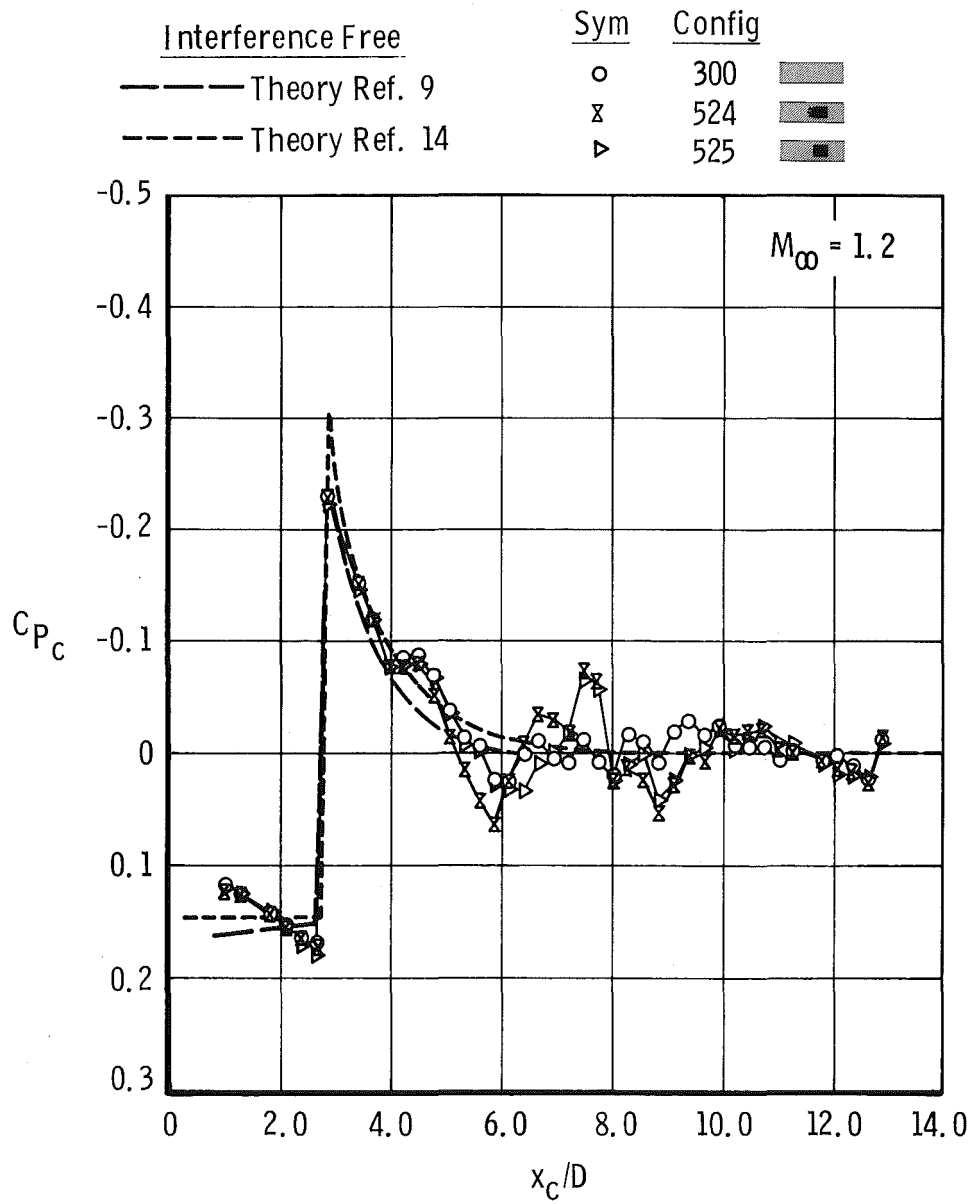
c. Window position
Figure 12. Continued.



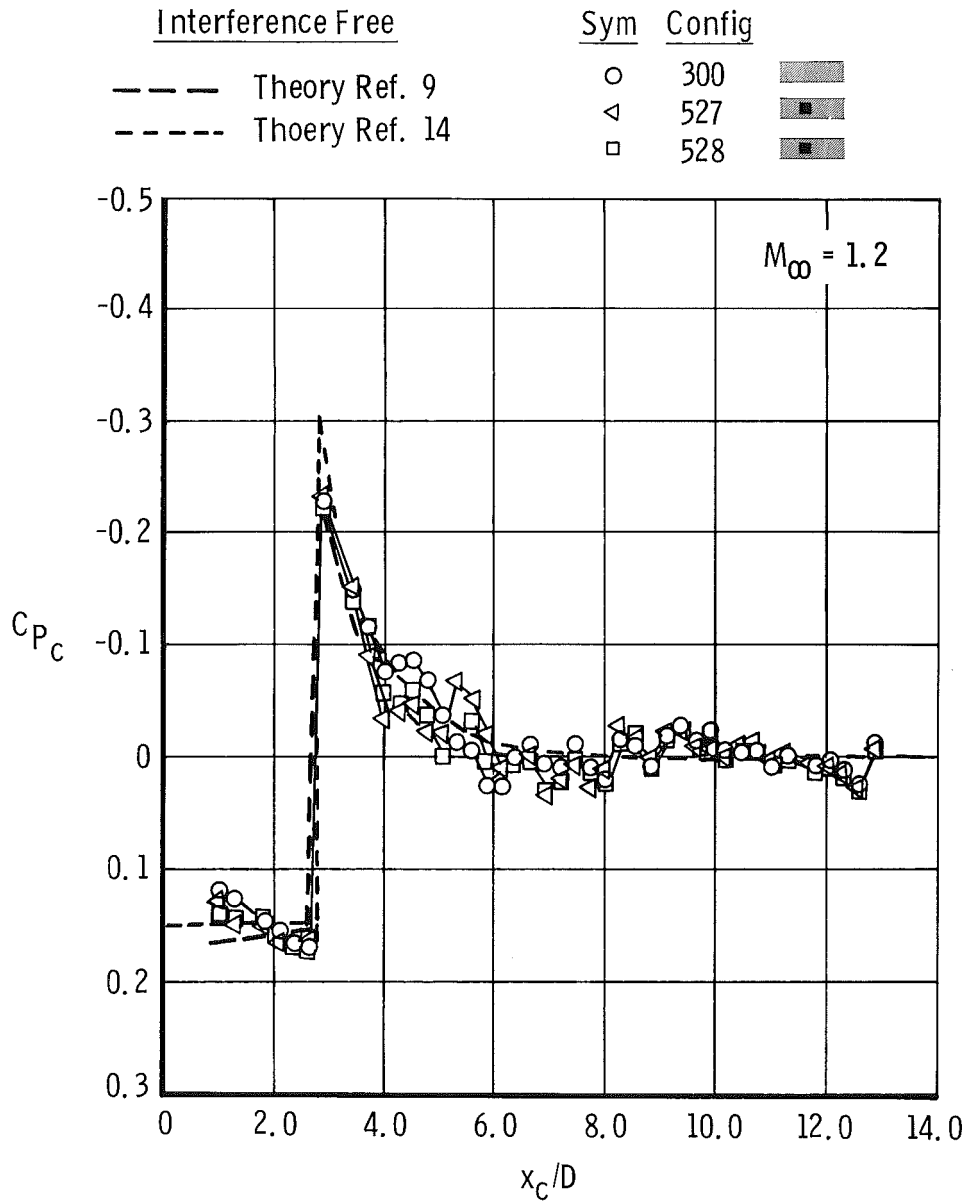
c. Concluded
Figure 12. Continued.



d. Forward transition region
Figure 12. Continued.

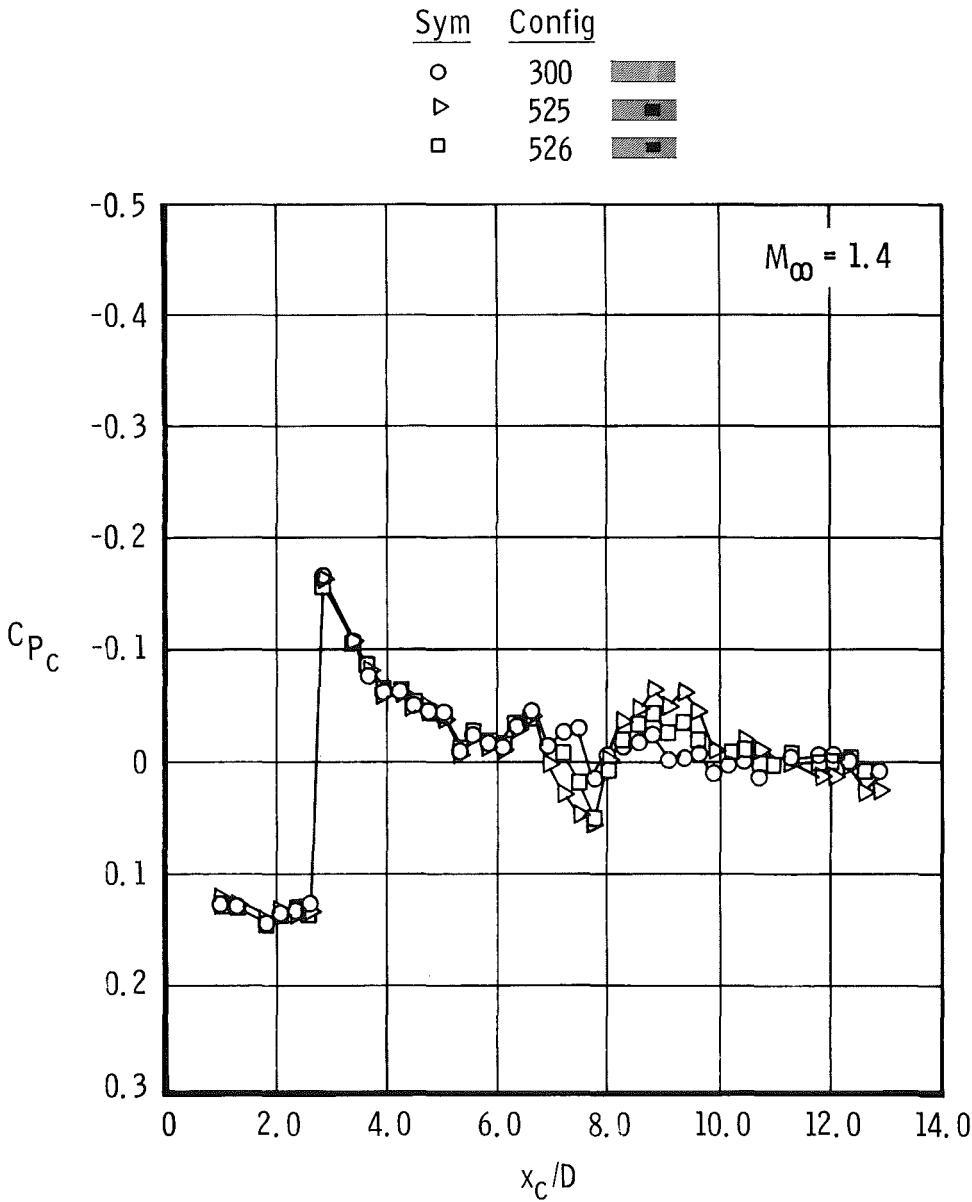


d. Concluded
Figure 12. Continued.

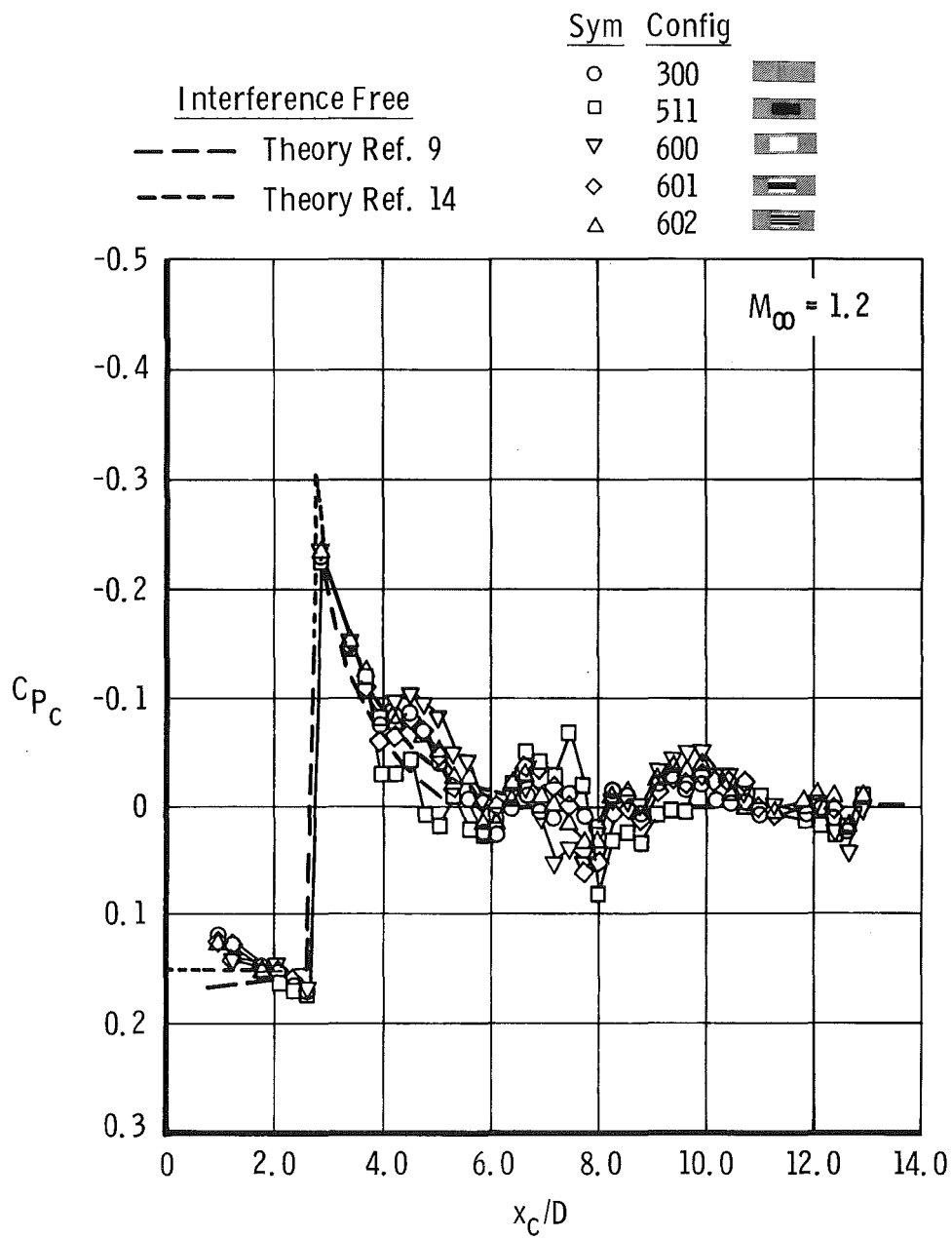


e. Strip window (aft position)

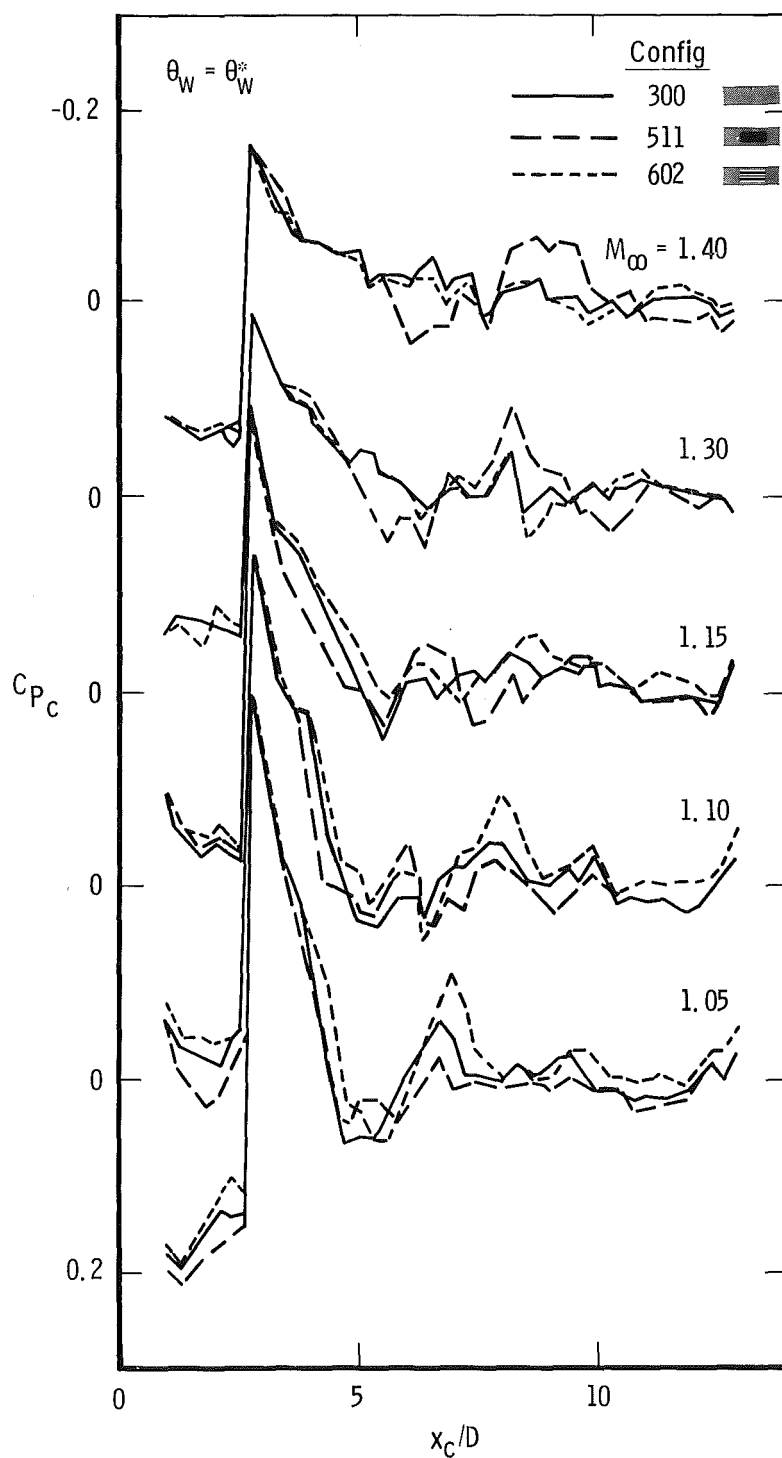
Figure 12. Continued.



f. Strip window (forward position)
Figure 12. Continued.

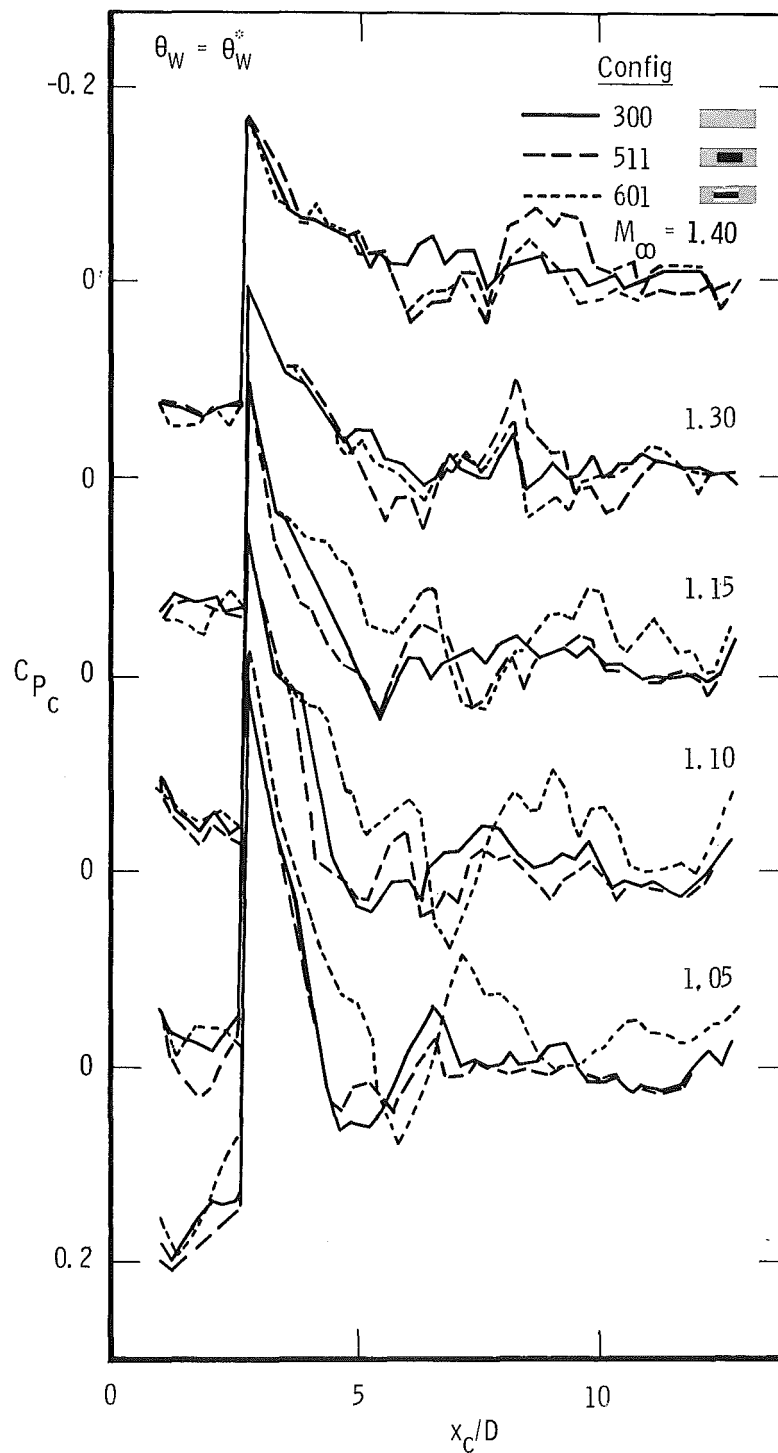


g. Constant average Q
 Figure 12. Concluded.

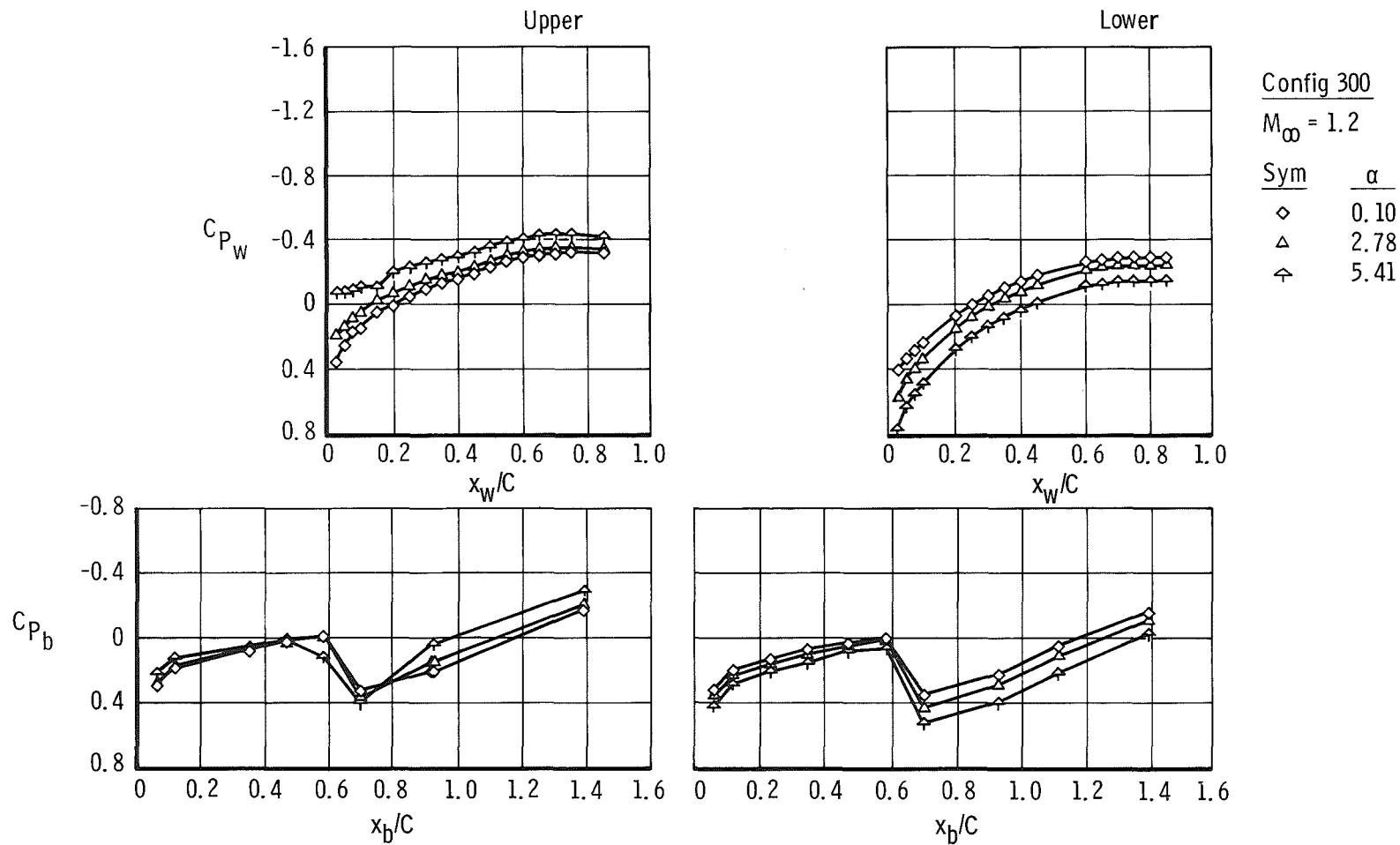


a. Strip window

Figure 13. Axial distribution of pressure coefficient on cone/cylinder for selected wall configurations and Mach numbers above 1.0.

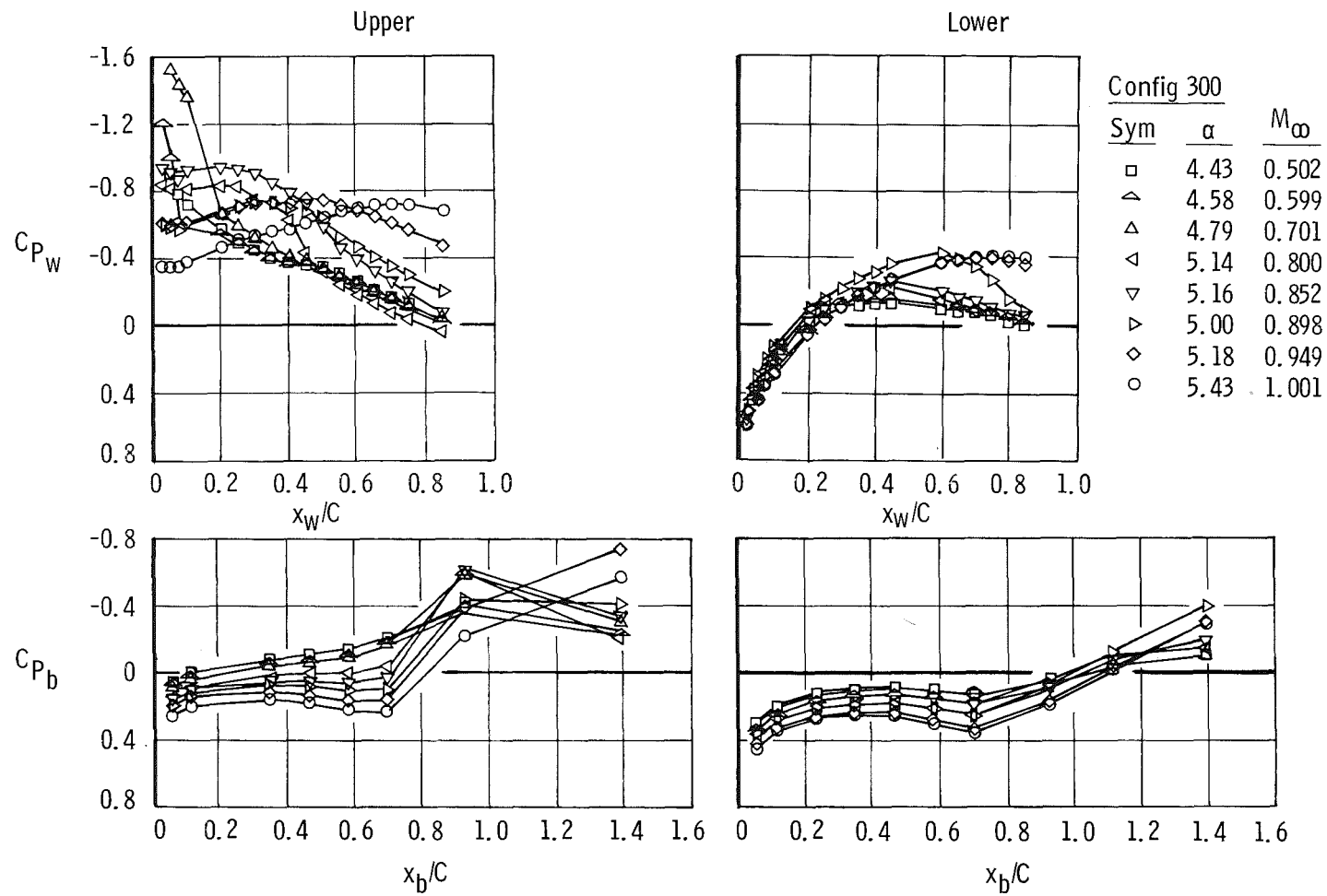


b. Single window
Figure 13. Concluded.

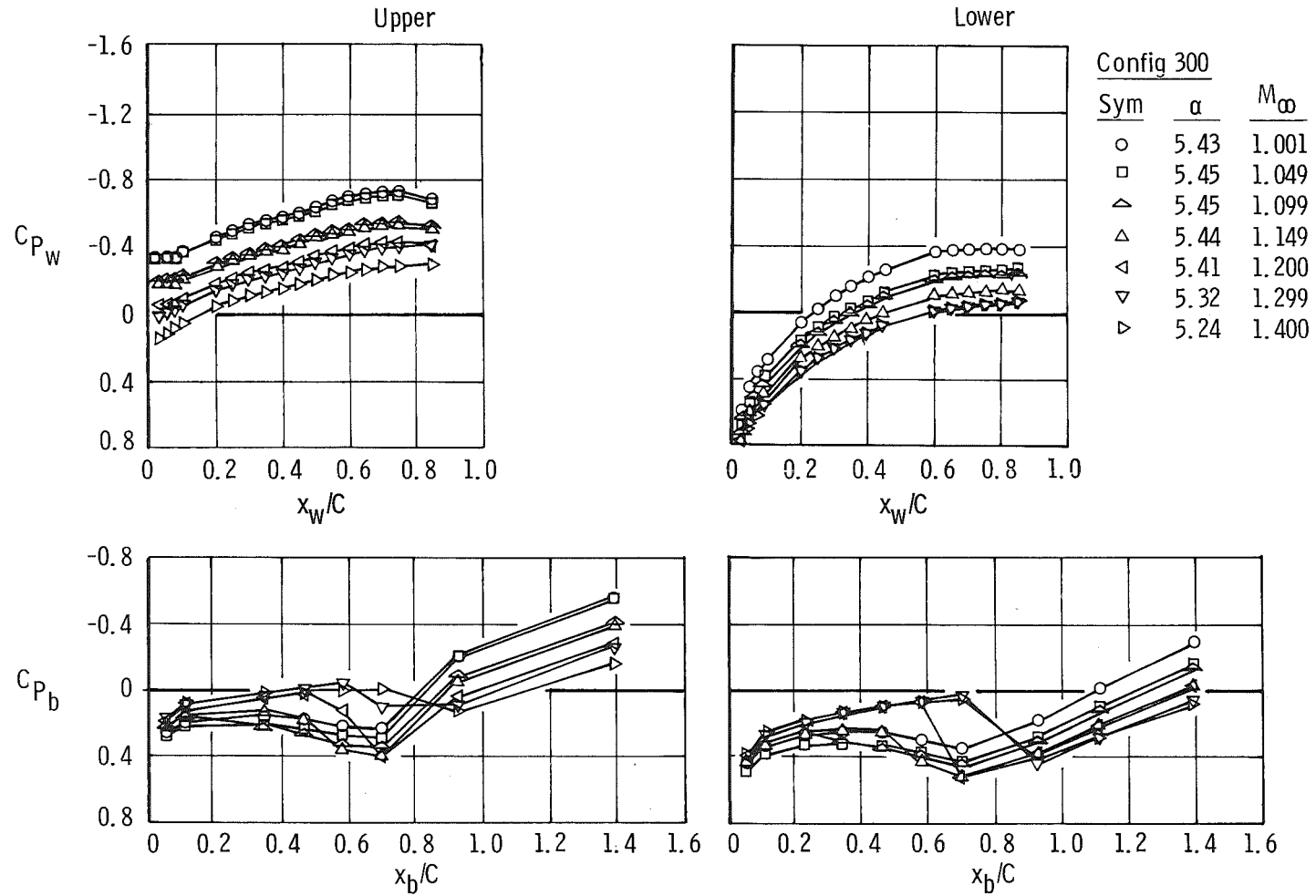


a. Effect of angle of attack

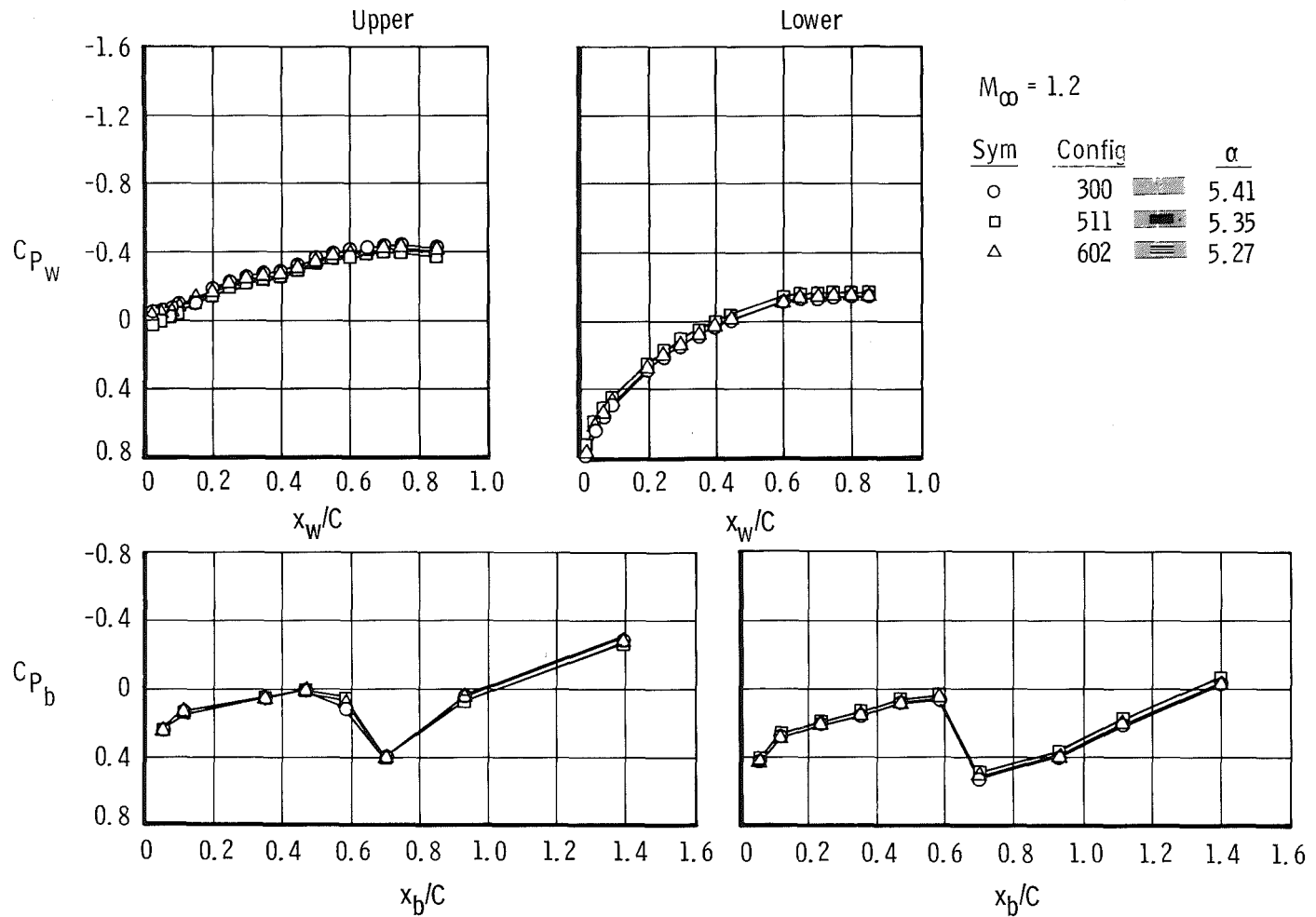
Figure 14. Distribution of pressure coefficient on the wing and centerbody for selected wall configurations and Mach numbers.



b. Effect of Mach number
Figure 14. Continued.



b. Concluded
Figure 14. Continued.



c. Effect of window configuration
Figure 14. Concluded.

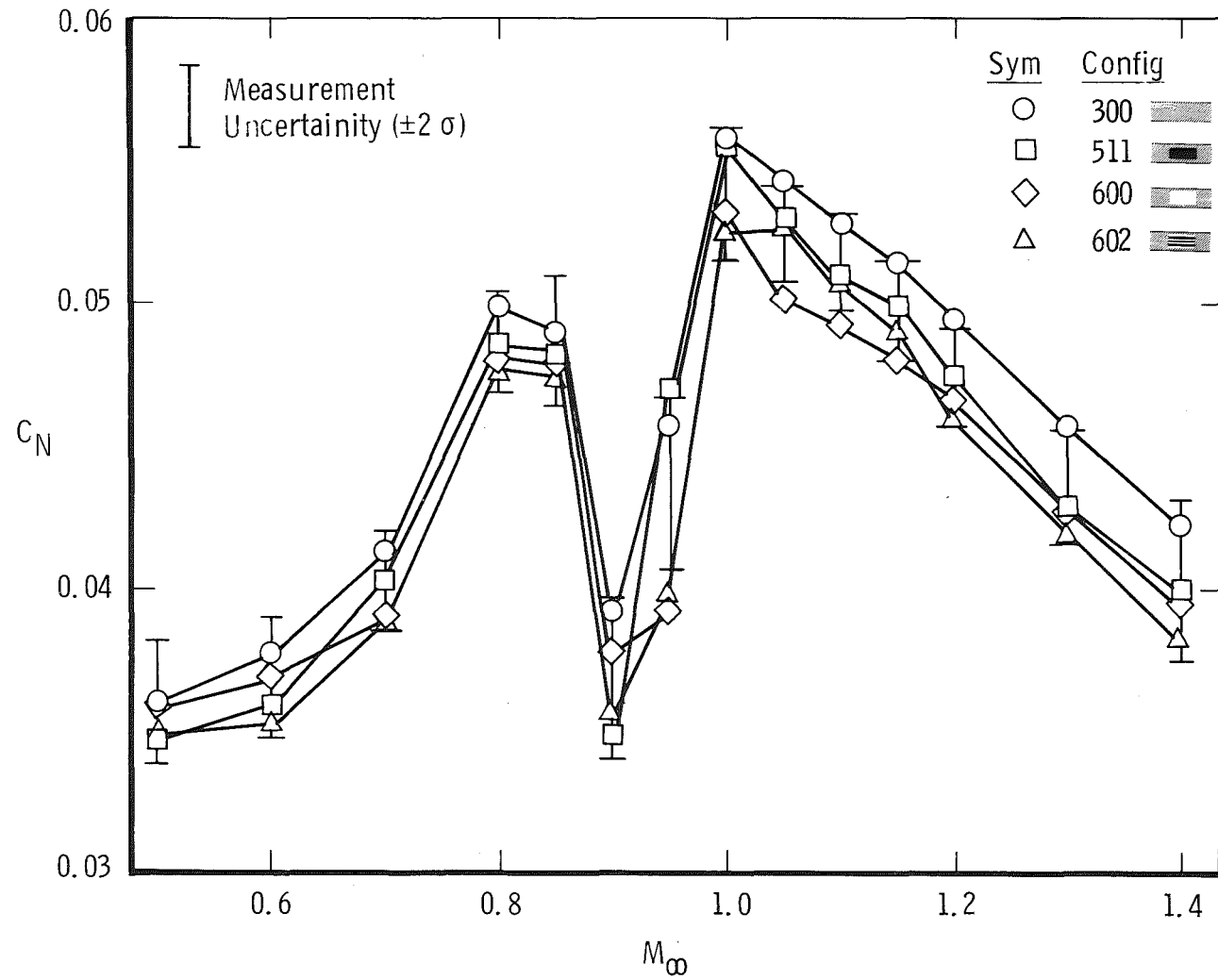


Figure 15. Variation of normal-force coefficient with Mach number, nominal $\alpha = 4$ deg.

NOMENCLATURE

b	Wind tunnel half-width, ft
C	Wing chord, ft
C_N	Normal-force coefficient
C_p	Pressure coefficient
D	Cylinder diameter, ft
F_N	Normal force, lb
h	Wind tunnel half-height, ft
M_∞	Free-stream Mach number
Q	Porosity parameter, $Q = 0$ is closed wall and $Q = 1$ is open jet
s	Half-span of vortex horseshoe, ft
u_∞	Free-stream velocity, ft/sec
v_i	Vector projection of local interference velocity, ft/sec
x	Distance along tunnel centerline from a disturbance, ft
x_b	Distance from centerbody nose, ft
x_c	Distance from cone/cylinder nose, ft
x_w	Distance from wing leading edge, ft
α	Angle of attack, deg
β	Compressibility factor, $(1 - M_\infty^2)^{1/2}$
δ	Lift interference factor at tunnel centerline
θ_w	Wall angle (positive when diverged), deg
θ_w^*	Optimum wall angle, deg
λ	h/b
τ	s/b

ρ Density, lb/cu ft

Ω_w Wake blockage ratio at tunnel centerline

SUBSCRIPTS

b Centerbody

c Cone/cylinder

w Wing